

Variations in cloud cover and cloud types over the ocean
from surface observations, 1954-2008

Ryan Eastman, Stephen G. Warren

Department of Atmospheric Sciences

University of Washington

Seattle, WA 98195

Carole J. Hahn

Department of Atmospheric Sciences

The University of Arizona

Tucson, AZ

Draft 8

Revised version returned to *Journal of Climate*, May 2011

Corresponding author address:

Ryan Eastman
Department of Atmospheric Sciences
University of Washington, Box 351640
Seattle, WA 98195-1640
tel. (206) 250-6296
fax (206) 543-0308
Email:
rmeast@atmos.washington.edu
sgw@atmos.washington.edu

Abstract

Synoptic weather observations from ships throughout the world ocean have been analyzed to produce a climatology of total cloud cover and the amounts of nine cloud types. About 54 million observations contributed to the climatology, which now covers 55 years, from 1954 to 2008. In this work interannual variation of seasonal cloud amounts are analyzed in 10-degree grid boxes. Long-term variations on the order of 5 – 10 years, coherent across multiple latitude bands, remain present in the updated cloud data. A comparison to coincident data on islands indicates that the coherent variations are probably spurious. An exact cause for this behavior remains elusive. The globally-coherent variations are removed from the grid-box time series using a Butterworth filter before further analysis.

Before removing the spurious variation, the global average time series of total cloud cover over the ocean shows low-amplitude, long-term variations on the order of 2 percent over the 55-year span. High-frequency, year-to-year variation is seen on the order of 1-2%.

Among the cloud types, the most widespread and consistent relationship is found for the extensive marine stratus and stratocumulus clouds (MSC) over the eastern parts of the subtropical oceans. Substantiating and expanding upon previous work, strong negative correlation is found between MSC and sea surface temperature (SST) in the eastern north Pacific, eastern south Pacific, eastern south Atlantic, eastern north Atlantic, and the Indian Ocean west of Australia. By contrast, a positive correlation between cloud cover and SST is seen in the central Pacific. High clouds show a consistent low-magnitude positive correlation with SST over the equatorial ocean.

In regions of persistent MSC, time series show decreasing MSC amount. This decrease could be due to further spurious variation within the data. However, the decrease combined with observed increases in SST and the negative correlation between marine stratus and sea surface temperature suggests a positive cloud feedback to the warming sea surface. The observed decrease of MSC has been partly but not completely offset by increasing cumuliform clouds in these regions; a similar decrease in stratiform and increase in cumuliform clouds had previously been seen over land.

Interannual variations of cloud cover in the tropics show strong correlation with an ENSO index.

1. Introduction

Earth's climate is dominated by the oceans. Clouds play important roles in climate, affecting both radiation fluxes and latent heat fluxes, but the various cloud types affect marine climate in different ways. Marine stratus and stratocumulus clouds (MSC) have an albedo of 30-40%, while maintaining a cloud-top temperature not much below the sea-surface temperature (SST) (Randall et al. 1984). MSC therefore have a cooling effect on climate (negative cloud radiative effect, CRE). Randall et al. (1984) estimated that a 4% increase in MSC cover could offset a 2-3°C global temperature rise. By contrast, high (cirriform) clouds are thinner and colder, so their longwave effect dominates, giving them a positive CRE.

Oceanic weather has been reported for many decades by professional observers on weather ships and military ships, but most of the observations come from volunteer observers on merchant ships. The number of reports per day from ships is only one-tenth as many as from weather stations on land. However, geographical gradients are smaller over the ocean than over land.

We have prepared a climatology of the distribution of total cloud cover and cloud type amounts over the global ocean, on a 5° x 5° latitude-longitude grid, as an update to supersede the cloud atlas of Warren et al. (1988). The updated climatology has more years of data, allowing better geographical coverage in sparsely-sampled parts of the southern hemisphere. It also obtains more accurate diurnal cycles by using only those night-time observations made under adequate moonlight. It groups the clouds into 9 types, instead of the 6 used in the 1988 atlas, in particular separately reporting amounts for each of the three low stratiform clouds: stratus, stratocumulus, and fog. The second-edition climatology consists of about 1000 maps, available on our website www.atmos.washington.edu/CloudMap, representing the seasonal and diurnal cycles of all cloud types averaged over the years 1954-1997. This paper's focus is on interannual variations in cloud cover. For the purpose of studying these variations, our database of seasonal and monthly cloud amounts for individual years has been updated with an additional 12 years of cloud data to cover the 55-year span

from 1954 to 2008 (Hahn and Warren 2007, updated 2009). This database has a coarser $10^{\circ} \times 10^{\circ}$ latitude-longitude grid compared to our climatology, but contains information on the same cloud types and base heights. To illustrate the potential uses of the database we show a few examples of correlations of selected cloud types with SST and ENSO, emphasizing the low stratiform clouds.

The relations between marine clouds and other environmental factors such as SST and lower-tropospheric stability (LTS) have been studied extensively for MSC. Norris and Leovy (1994), using surface observations from our earlier databases, found a negative correlation between SST and MSC in midlatitude oceans, strongest during summer and strongest for MSC lagging SST. They also noted the transition from stratiform to cumuliform clouds in regions with strong gradients of SST, with stratiform clouds on the cool side. Wyant et al. (1997) used a two-dimensional eddy-resolving model to study the equatorward transition from stratiform to cumuliform clouds. They found that rising SST acts to destabilize the marine boundary layer, eventually leading to the entrainment of dry air into the cloud deck and the replacement of stratus cloud with cumulus. Bony and Dufresne (2005) showed that a breakup of marine cloudiness in regions of subsidence produces a strong positive feedback between shortwave (SW) cloud radiative effect and SST. They go on to say that models do not agree well with observed relationships between SST and SW CRE, and that predictions of how this feedback will evolve with increased greenhouse gas forcing differ significantly between different coupled models.

The influence of SST on low cloud cover may be by means of lower tropospheric stability (LTS), which correlates negatively with SST. Klein and Hartmann (1993) showed that in regions where MSC is persistent the greatest cloud cover occurs during the season of highest LTS. Wood and Hartmann (2006) also found that higher cloud fractions occurred when LTS was greater. Clement et al. (2009) showed that lower LTS goes with higher SST in the NE Pacific, concluding that total cloud cover is reduced when SST warmed. These studies have produced a consistent finding that reduced LTS can be caused by increasing SST, which causes a decrease in cloud fraction by initiating a tradeoff from stratiform to cumuliform cloud cover. Clement et al. (2009) showed a shifting pattern in the NE

Pacific, with cool SST, higher LTS, and greater coverage of MSC from 1952 through 1976, then again from 1996 through the end of the observed period in 2005.

Decadal trends in marine low clouds from surface observations were judged by Bajuk and Leovy (1998) to be mostly spurious. Using cumulonimbus as an example they showed a long-term, low-frequency variation that was coherent across nearly every 10° latitude band and not explained by any known physical mechanism. A possible explanation for this behavior was put forth by Norris (1999), proposing that as economies change the number of ships originating in different countries also changes, causing subtle shifts in observing procedures over time. However, he did not find evidence to support this hypothesis, so an explanation of the observed coherence remains elusive. To discount the low-frequency variations, Norris (2000) recommends studying surface-observed marine clouds in terms of interannual variations or on small scales rather than looking for multidecadal trends on zonal or global scales.

Trenberth and Fasullo (2009) examined global climate models for their changes in Earth's radiation budget between 1950 and 2010. The models were those used in the Fourth Assessment Report of the Intergovernmental Panel on Climate Change (IPCC). Their assessment concludes that significant surface warming is expected due to decreasing global cloud amounts. Specifically, they predict a decrease of low and middle clouds in mid-latitudes, and a decrease of high clouds near the equator. Increases of cloud cover are predicted over the poles. Significant changes are predicted over both land and ocean; the largest predicted changes are over land and over the Arctic.

The goal of this paper is to use our updated surface-observed cloud dataset, spanning 1954 to 2008, to analyze interannual variations in total cloud cover and nine cloud types over the ocean. We will investigate the tendency observed by Bajuk and Leovy for different zones to vary coherently and we will attempt to remove this bias prior to further analysis. The relationship between SST and cloud cover will be studied on local and global scales for several cloud types. Other causes for variability of cloud amounts, such as El Niño, will also be investigated. The structure of this paper parallels our

paper on cloud changes over land (Warren et al. 2007); the methods of analysis used in both papers are explained in more detail in the 2007 paper.

2. Data

Cloud data for this study come from weather reports taken aboard ships and reported in the synoptic code of the World Meteorological Organization (WMO, 1974). The observations are then further processed to form the Extended Edited Cloud Reports Archive (EECRA, Hahn and Warren 1999 (updated 2009)). Figure 1 shows the number of usable cloud observations taken per year. A decline in reporting has taken place since 1985. Original ship reports were taken from the International Comprehensive Ocean-Atmosphere Data Set (ICOADS, Woodruff et al., 1987, 1998; Worley et al. 2005). Cloud reports in the current version of the EECRA span the period 1954 through 2008 over the ocean and from 1971 to 1996 over land. An update of the land data through 2008 is underway; it was used in the Arctic analyses of Eastman and Warren (2010a,b). ICOADS contains many ship observations from decades prior to the 1950's, but we begin our analyses in 1954. This is because a major change in the classification of cloud types was instituted in 1949, and it was not until 1954 that the change was adopted by ships of all nations.

Cloud reports from ships are generally made at 3 or 6 hour intervals, usually at UTC hours divisible by 3, giving 4 or 8 cloud observations per day per ship. Cloud reports stored in the EECRA contain information about cloud amount and type at three levels: low, middle, and high. The present-weather code is used when necessary to assign the cloud type (particularly precipitating clouds and fog). Also stored are variables concerning illumination of the clouds by sunlight, twilight, and moonlight: solar zenith angle, lunar illuminance, and a "sky brightness indicator". The sky brightness indicator is given the value of '1' if the combined solar and lunar illuminance satisfied the criterion recommended by Hahn et al. (1995), which corresponds to a full moon at 6° elevation or a half moon at zenith; otherwise it is assigned a '0'. For our climatology day and night cloud reports are not

determined by this brightness indicator, but instead by local time. Daytime observations are those taken between 06:00 and 18:00 local time, and night observations are those from 18:00 through 06:00. As will be discussed later, only daytime cloud reports are used in this study, and among those reports only those with brightness indicator values of 1 are used.

The synoptic code defines a total of 27 cloud types, 9 for each of 3 levels (WMO 1956, 1974). For our analysis we have grouped the clouds into nine groups: five low, three middle and one high. The amounts of middle and high clouds are less reliably determined than those of low clouds because they are often partially or totally obscured by lower clouds; we obtain their frequencies of occurrence from a subset of observations in which their level was observable (Hahn and Warren 2003). We define the upper levels as observable only when there is 6/8 or less low cloud cover. Table 1 lists the nine cloud groups we distinguish, together with our computation of their global average amounts, and base heights for the low clouds. For some purposes in this paper we combine two or three cloud types; in particular "MSC" is the sum of stratus (low cloud types 6 and 7), stratocumulus (low cloud types 4, 5, and 8) and fog (from the present-weather code).

For our long-term average climatology, we report seasonal cloud amounts on a $5^\circ \times 5^\circ$ latitude-longitude grid (with coarser longitude intervals at higher latitude to maintain approximately equal-area grid boxes). The climatology is available as maps on our website www.atmos.washington.edu/CloudMap, from which digital values can also be downloaded. In most parts of the ocean there are not enough cloud observations to form reliable seasonal averages on a 5° grid for individual years, so our investigation of interannual variations and trends in this paper uses a coarser grid, $10^\circ \times 10^\circ$ (1100 km on a side at the equator). At latitudes poleward of 50° the longitudinal span of gridboxes is increased to maintain approximately equal-area boxes, similar to the 5° grid. This means that for latitude zones near the poles there are fewer boxes per zone.

Within a grid box, two seasonal or monthly average quantities of cloud cover are formed: The amount when present, defined as the average fraction of sky covered by a particular cloud type when it

is present; and the frequency of occurrence, defined as the number of times a cloud type was reported divided by the total number of reports in which its level was visible. Middle and high clouds are often hidden from view by a lower overcast cloud; the frequency and amount-when-present of these clouds were formed using adjustments that are described in our earlier papers (e.g. Warren et al. 2007; Warren and Hahn 2002). Seasons used are December, January, February (DJF); March, April, May (MAM); June, July, August (JJA); and September, October, November (SON). To form a seasonal average cloud amount, the frequency of occurrence is multiplied by the amount when present for that particular season. Further documentation on the calculation of averages is available in Warren et al. (2007). Using this 10° grid and the previously described methodology, gridded climatologies for total cloud cover, clear sky frequency, and amounts of nine cloud types have been created. Documentation for the land and ocean climatologies is available in Hahn and Warren (2007).

Some examples of time series of total cloud cover for individual seasons within 10° boxes for daytime are compared to time series for nighttime in Figure 2. Seasonal values are shown as well as the standard deviation of the seasonal means. These plots illustrate the year-to-year variability as well as the geographic variability of cloud cover. Cloud cover over the South Atlantic Ocean is consistently high at 80-90%, whereas cloud cover in Indonesia (ocean area only) in SON is much more variable and only ~50% on average (Figures 2k, 2l). A box in the central equatorial Pacific (Figure 2i) shows occasional years with much greater cloud cover than normal; these correspond to ENSO events.

It is apparent in Figure 2 that many more years are represented for daytime than for night; this is because only ~38% of nighttime observations satisfy our criteria for adequacy of illuminance. In sparsely sampled boxes, sufficient numbers of observations to form a reliable average may be available for daytime but not for night. In our global climatology (www.atmos.washington.edu/CloudMap), cloud amounts are calculated separately for day and night. A day/night average is also formed using the average of the day and night cloud amounts (day amount + night amount) / 2. If there are insufficient cloud observations during the day or night, the average of all observations is used. If there

are very few observations during the night but sufficient daytime observations, the daytime average is used as the day/night average. In most of the examples in Figure 2 the day and night seasonal variations in cloud cover appear to be related. Figure 3 shows how the daytime cloud anomalies compare with night anomalies for all grid boxes for all cloud types, using DJF as the example season. The r-squared value from the linear correlation between the day and night anomalies is shown for each plot. The correlations are all significant; the best correlation (aside from total cloud cover) is for stratus and stratocumulus. Only daytime values are used in the analyses below, in order to avoid any day/night sampling biases. [The analyses were also done using the day/night averages, and very similar results were obtained.]

The computed seasonal average cloud amount for a grid box in a single year is more accurate if a large number of observations enter the average, so we have to set a criterion for the minimum number of observations required to form an average. Also, the significance of correlations is limited by the number of years available in the time series. However, if the criteria chosen are too strict, the areas for which results can be obtained will be limited to regions of heavy ship traffic. So the minimum number of observations (minobs) required to form a box-average cloud cover must be high enough to ensure that observed variation is real, but a lower minobs greatly increases the number of grid boxes available for study. Figure 8 of Warren et al. (1988) shows that to reduce RMS error to below 5%, roughly the computed standard deviation shown in Figure 2, a minimum of 25 observations must be present to form an average cloud amount for a particular season.

When forming a time series for a large area by averaging time series from individual grid-boxes, we ensure that time series are representative of the entire time period by requiring that at least three years of data be present within each 11-year span: 1954-1964, 1965-1975, 1976-1986, 1987-1997, 1998-2008 in each grid box. When cloud data from individual boxes are used in a linear correlation we also require representation from each decade and the minimum number of required years remains at 15, which means that any r-value above 0.44 is significant at a 90% level.

Cloud data are compared with other data in this study. Additional data sets include the NCEP/NCAR reanalysis data (Kalnay et al. 1996), the UK Met Office HadISST1 SST dataset (Rayner et al. 2003) and ENSO data, produced by the Japanese Meteorological Agency, using methods described by Meyers et al. (1999).

3. Analysis of global time series

The global average cloud amounts in Table 1 show some striking differences between land and ocean. The ocean is cloudier than the land, with average total cloud covers of 68% and 54% respectively. It is particularly the low clouds that are much more common over the ocean. In addition, the base heights of these low clouds are lower over the ocean; this is likely due to the higher humidities at the water surface.

The only cloud type that has greater coverage over land is cirriform cloud. Is this a real difference, or is it instead the result of a difficulty to observe high clouds over the ocean, where the low clouds are more prevalent than over land? In our analysis procedure we used a method that was intended to remove biases due to obscuration by underlying clouds by using the random-overlap assumption (Warren et al. 2007); this allowed us to compute the total amounts of high clouds, including the portions hidden by lower clouds. The land-ocean difference in cirrus amount could result from inaccuracy in this procedure, since it is likely that the co-occurrence of high and low clouds is not random. Another reason for the difference is that the optical depth required for cirrus to be visually apparent is probably greater over the ocean due to widespread sea-salt haze in the marine boundary layer. Alternatively, the cirrus amount may truly be greater over land, where orographic gravity waves can produce high clouds over or near mountain ranges or other terrain features.

Figure 4 shows, for several cloud types, the global annual average cloud amount anomaly (black line) as well as the annual average anomaly time series for each 10° latitude zone (gray lines). Global and zonal seasonal anomalies in percent cloud amount are computed using the criterion outlined

in the data section, with individual grid-box anomalies weighted by relative box size and percent ocean, then averaged to form yearly anomalies. In Figure 4 the zonal time series have been scaled to the zonal average amount of each cloud type, similar to the method used by Bajuk and Leovy (1998), but using anomalies instead of amounts. The scaled zonal anomaly $A'_i(t)$ is computed for each cloud type by multiplying the raw zonal anomaly $A_i(t)$ by the ratio of the global average cloud amount, \bar{c}_{glo} over the zonal average cloud amount \bar{c}_i , as shown in Equation 1. This method allows fluctuations to be compared in zones with different average cloud amounts.

$$A'_i(t) = A_i(t) \frac{\bar{c}_{glo}}{\bar{c}_i} \quad (1)$$

Total cloud cover appears to be steadily increasing in Figure 4a until 1998, when the time series begins a declining trend. The same pattern is amplified in low-cloud amount in frame b. The pattern in total cloud cover is therefore likely caused by low clouds. Middle cloud cover shows a tendency to fluctuate in opposition to the low-cloud cover time series, though the peak in low clouds occurs five years prior to the low-point in the time series of middle clouds. A peak in middle clouds is seen in 1988. It is possible that middle-cloud changes are acting to offset the effects of low clouds on the total cloud cover time series. High cloud amount shows just a steady climb since 1967. The total high-cloud change is + 5% on an average of 12% (Table 1), which means a surprisingly large relative change of 40%. This substantial trend does not agree with the satellite-derived trend in high clouds shown by Wylie et al. (2005) Though we require the upper levels to be at least 2/8 visible, it is possible that the random overlap assumption can introduce a bias in the time series of middle or high clouds given diurnal, seasonal, or decadal-scale variations in lower cloud cover. Deviations from random overlap are discussed by Warren et al (1985). Because of this, we focus on interannual variations of low cloud cover in this paper.

Time series of stratiform and cumulus clouds are shown in Figure 4e-h. Stratus and Sc amounts are nearly constant from 1954 through 1980 and thereafter show greater variability. After the year

2000 St and Sc show strong opposing behavior, which could result from a subtle change in observers' distinction between these two types. Because of this sudden opposing behavior we have combined the two stratiform types in the time series in the third frame, where the plot is more flat after 2000. The combined stratiform plot shows a distinct rise and fall between 1990 and 2000, and the plot of cumulus clouds (fourth frame) shows a similar rise and fall somewhat later, between 1995 and 2005. These two types do not appear to be 'trading off' globally. Combined, they do explain the rise in low cloud amount between 1990 and 2005 seen in Figure 4b.

4. Discussion of time series; removal of spurious decadal-scale variations

The plots in Figure 4 exhibit the coherent behavior between latitude zones pointed out by Bajuk and Leovy (1998, hereafter BL98). Cloud amount in most 10° latitude zones (gray lines) tends to follow the global mean (black line) through the period of record. Global and zonal cloud cover anomalies deviate from zero by as much as four percent for periods of 10 to 20 years. This behavior was not attributed to any natural causes or dataset-related issues by BL98, though possibilities were put forth in their work, including subtle changes in observing procedure over time or a change in the fractions of nations contributing ship reports. Norris (1999) investigated those hypotheses, but could neither substantiate nor rule out either possibility. No natural explanation for such behavior has been identified, and the variations do not appear to show any trade-off of cloud types over time. Such a trade-off could either be physical or a symptom of a change in observing procedure. Of course, a change in procedures in only one nation would not be as apparent in the ocean as it is on land, because ships of many nations sample each oceanic grid box. A similar analysis was done using data from weather stations on land (Warren et al. 2007), and no such coherence was observed for the period 1971 to 1996.

We have devised a test comparing cloud observations taken on ships to those taken on islands to determine whether geographically coherent variations in ocean cloud cover are also seen by land

observers. A region was chosen in the central Pacific Ocean, outlined in Figure 5, where observations at weather stations on islands (in most cases on the coasts of these islands) coincide with those taken on ships. Separate time series representing island and ship observations for multiple cloud types were developed for this region. Each time series was decomposed into two contributions: (a) the long-term variation on the order of 5-10 years captured by a Butterworth (low-pass; Hamming, 1989) filter; and (b) the residual; i.e. the difference between the long-term variation and the actual time series, chosen to represent the high-frequency, year-to-year variation in cloud cover. Only cloud data for the period 1971 through 1996 are used, when surface observations over both land and ocean are available. If these coherent variations are real, we expect to see the long-term variations for island-observed clouds match those for ship observations. This match will be meaningful provided that the high-frequency variation shows similarity, indicating that some year-to-year cloud variations are seen both from ships and from island stations.

Time series of seasonal cloud-type anomalies observed from ships and islands in the central Pacific are shown in Figure 6 along with the filtered, long-term variations. Long-term variation was also quantified using a 5th-degree polynomial fit, producing nearly identical results. Island-observed clouds are plotted in gray; ship-observed clouds in black. Both land and ocean time series for every type show variation at decadal or greater time scales. Long-term variation is not consistent between ocean and land, however, as the smooth curves produced by the filter appear to be unrelated in most cases. The residuals, however, are positively correlated as shown in Figure 7. For all types but cumuliform the correlations are significant at a 96% level or greater. It is not surprising that cumuliform clouds would show the weakest relationship between islands and ocean, because of their small size and due to the land-sea interactions that can form cumulus clouds over islands, but not over the water, or vice-versa. Significant positive correlation between the residuals indicates a low probability that the residual time series coincide by chance. It is likely, then, that island and ship observers are seeing *some* of the same clouds. A comparison of decadal-scale variations in cloud cover

does not suggest agreement between island and ship observations. This provides evidence that the long-term, latitudinally coherent variations first shown by BL98 are spurious.

Time series of the global average anomaly of total cloud cover are shown in Figure 8 for land and ocean separately. For Figure 8, no attempt has been made to remove the long-term variation over the ocean discussed above. The two time series exhibit small changes that appear to be opposing one another between 1971 and 1996, the period when the data overlap. Initially, the two time series were significantly anti-correlated, a surprising result. However, after a Butterworth filter was used to remove long-term variation during the coinciding time period, no correlation between the interannual variations was observed. Figure 8 shows that the global average cloud cover has been remarkably stable for half a century in spite of changes in global average temperature. Kato (2009) postulated a negative feedback on global cloud cover tending to maintain a constant global average albedo; the near-constancy shown in Figure 8 may support Kato's hypothesis.

The previously discussed spurious correlation highlights the need to distinguish between long-term and short-term variability in cloud-cover time series. When correlating time series or looking for trade-offs in cloud types, it is best to remove the long-term variability in order to reduce the possibility of spurious correlation. For the remainder of this study, all time series used in linear correlations will employ a low-pass Butterworth filter (identical to that used in Figure 6) to subtract long-term variation from individual time series, forcing the correlations to be for year-to-year variation only. A polynomial fit was also employed to remove the variation, producing nearly identical results.

5. Variations of marine cloud cover correlated with temperature and ENSO

It has been shown by numerous studies (Norris and Leovy, 1994; Wyant et al., 1997; Clement et al., 2009) that marine stratiform cloud cover should and does correlate negatively with SST. The hypothesized mechanism for this relationship is a destabilization of the lower troposphere by the warming SST, reducing static stability and entraining more dry air into the cloud layer. In this section

we will test this hypothesis using filtered data, where long-term variation is removed from all time series by a Butterworth filter. Data will span the length of our studied time period, from 1954 through 2008. Correlations shown are between anomalies calculated for all individual seasons (four per year). We correlate cloud-cover variations with variations in SST, as well as lower tropospheric stability (LTS, $\Theta_{850} - \Theta_{1000}$ and $\Theta_{700} - \Theta_{1000}$, where Θ is potential temperature), surface relative humidity (RH), sea level pressure (SLP), and surface air temperature (SAT). We have chosen to examine RH and SLP in order to show how other meteorological variables influence marine cloudiness besides stability and SST. RH quantifies the available moisture, while SLP should give a measure of the strength of subsidence, which should correlate with LTS. Actual numerical values of correlations are less meaningful because these variables are not independent, instead broad consistent patterns in different regions are considered better indicators of significance. Values for LTS, RH, SLP, and SAT were taken from the NCEP/NCAR reanalysis dataset (Kalnay et al. 1996).

Sea-surface temperature, based on the UK Met Office HadISST1 dataset, is correlated with total, low, and high cloud cover in Figure 9. Correlations are shown as dots, with the dot size indicating the strength of the correlation, dark dots representing anti-correlations, and white dots representing positive correlations. Dots surrounded by gray represent correlations significant at the 99% level. The three maps indicate that low clouds are more strongly correlated with SST than are high clouds. The pattern of correlations shown for total cloud cover closely matches that for low cloud cover. Colder ocean water is associated with increased low cloud amount in regions of persistent MSC, such as off of the SW coast of North America, the west coast of South America, the SW coast of Africa, the coast of southern Europe, and the west coast of Australia. Low clouds correlate positively with SST over regions of warm SST, as is shown by the patches of positive correlations over the Indian Ocean, the central Pacific, the western Pacific warm pool, and the Caribbean. High clouds increase with SST in the equatorial Pacific but elsewhere show little correlation except for a weak positive correlation in the Arctic. Maps of correlations between cloud anomalies and variations in SAT (from

NCEP/NCAR reanalyses) instead of SST showed nearly identical patterns in all three frames.

In Figure 10, daytime seasonal anomalies of MSC and cumulus cloud amounts are plotted against SST anomalies. All time series had long-term variation removed by the Butterworth filter before they were plotted. The region represented is the southeast Atlantic, west of southern Africa, where low clouds correlate negatively with SST. This is region 5 in Figure 11. Best-fit lines are calculated using a least squares regression which takes error in both axes into account (Press et al. 2002, section 15.3). Error ellipses for each point were calculated based upon the number of cloud observations taken that season. Details of this method are outlined in section 11a of Warren et al. (2007). The two scatter-plots in Figure 10 show that as SST warms in this region, MSC decreases and Cu increases. In this particular figure MSC decreases much more than Cu increases, creating an uneven tradeoff and a net decrease in low cloud cover as SST warms. Similar plots were made for other regions of persistent MSC, regions 1-4 in Figure 11, all with similar results.

Besides SST, other variables such as LTS ($\Theta_{850} - \Theta_{1000}$), RH, and SLP also affect (and are affected by) MSC. Table 2 shows correlations of these variables with MSC and cumulus clouds as well as the correlations of these variables with each other. Regions chosen for the table are shown in Figure 11. Regions 1-5 were chosen because they showed significant negative correlation between stratiform clouds and SST over large, coherent areas. Region 6 was chosen because it showed a significant, positive correlation between clouds and SST over a coherent area. Each correlation is based upon 220 individual seasons of data (Four seasons per year of our 55-year span), meaning any correlation greater than ~ 0.2 in magnitude is significant at the 99% level. Numerical values of the correlations should not be given much weight however, since none of the variables are independent and measurement techniques (especially upper air data) are not consistent. Instead, the goal of this table is to highlight the inter-regional consistency and complexity of the climatological system surrounding MSC.

This table indicates that in the areas showing a negative correlation between SST and MSC, SST and LTS consistently have the strongest relationship with variations in MSC. SST is negatively

correlated with MSC at the 99% significance level and LTS is positively correlated with MSC at the 99% level except in region 1. For LTS, we also used $\Theta_{700} - \Theta_{1000}$, which produced similar results. As expected, cumulus shows significant opposite relationships with SST and LTS compared to MSC. Lower surface RH tends to favor cumulus more than MSC, while higher SLP favors MSC over cumulus in regions 2-5. In region 6 the relationship between cumulus clouds, stratiform clouds, and SST is opposite to the other regions. The correlations between LTS and cumulus/stratiform remain qualitatively the same as the other regions, though they are weaker in region 6. RH and cumulus again correlate negatively, while RH and stratiform clouds correlate positively. SLP correlates negatively with stratiform clouds, in contrast to regions 1-5.

Linear correlations between total cloud cover and ENSO are shown, again as dot plots, in Figure 12. The patterns shown in these plots are very similar to those published by Park and Leovy (2004). Changes in cloud cover, likely related to the changes in SST (and therefore lower tropospheric stability) and tropical circulation associated with ENSO, are evident over the entire equatorial Pacific. A positive ENSO brings about warmer SST and more cloud cover in the central Pacific, and reduced cloud cover over the Indonesian region as well as reduced cloud cover in the eastern Pacific. The cloud response to ENSO is most pronounced in DJF and SON and least pronounced during JJA. Cloud cover is reduced in the Indonesian region. Secondary effects away from the equatorial Pacific, likely the result of changes in global circulation associated with ENSO as suggested by Park and Leovy (2004), are also observed in all seasons in regions such as the Caribbean, the north Atlantic as well as the Indian Ocean.

6. Relation of ocean clouds to sea-surface temperature and observed changes

In regions of persistent stratiform clouds (regions 1-5 in Figure 11) correlations of low cloud cover anomalies with a variety of variables suggest that stratiform clouds in these regions are associated with a cool sea surface, higher RH, stronger stability, and higher sea level pressure. A

mechanism behind this relationship was hypothesized by Wyant et al. (1997), whereby an increase in SST causes a reduction in lower tropospheric static stability. The reduced stability allows for more vertical motion within and around the cloud deck, leading to increased entrainment of dry air. This brings about a reduction in cloudiness and a transition from stratiform to cumuliform cloud types. Higher SLP could also produce more subsidence aloft, increasing LTS independent of SST. When time series of seasonal stratiform and cumuliform cloud anomalies were correlated with each other in regions 1-6, a consistent negative correlation was seen. This relationship was unique between low stratiform and cumuliform cloud types, suggesting that these two types tend to trade off, meaning that in a given year or season one type is consistently more common at the expense of the other.

Plots correlating temperature to cloud amounts in the style of Figure 9 were done with other measures of temperature, including surface air temperature and LTS. The magnitude and distribution of correlations shown in Figure 9 did not significantly change when these other measures of temperature were used, aside from the expected sign change with LTS. Combined with the results of Table 2, this further substantiates the claim made in the introduction that SST and LTS are linked and that this proposed mechanism for observed cloud changes is sound, though other factors such as SLP (associated with circulation and meteorology) are certainly also influencing the clouds.

In an attempt to further scrutinize the observed cloud and SST behavior, the de-seasonalized time series of stratiform cloud cover for each region (1-6) are compared in Figure 13. The globally coherent variation in stratiform cloud cover is removed from each time series. The variation is first calculated using a low-pass filter on the global time series such as those shown in Figure 4. It is then scaled to the average stratiform cloud amount in each region and subtracted from the time series. The plots in Figure 13 show anti-correlation between SST and MSC in regions 1-5 as well as the positive correlation in region 6. Also hinted at in the plots is a decrease in MSC accompanied by an increase in SST in regions 1-5. Given the mysterious nature of the long-term variation in cloud cover found on the large scale, it is wise to be somewhat suspicious of the decrease of stratiform cloud cover. It was

initially reported by Norris (2002), though the results were never published.

If the decline in MSC were real, it would be expected that other variables associated with MSC would be changing in a complementary manner. In order to test the validity of these decreases in MSC we have applied linear fits to the time series of the variables correlated in Table 2. Table 3 shows the magnitude of these linear fits, which are calculated using the median-of-pairwise-slopes method of Lanzante (1996).

In regions 1-5, where stratiform clouds are decreasing, SST is slightly increasing. However, according to the reanalysis data, LTS along with RH and SLP are increasing in these areas, not consistent with the observed changes in cloud cover. Further investigation would be required to sort out this inconsistency; as some of the variation in the reanalysis data may be spurious.

If spurious variation were still affecting the cloud data, we would expect it to be shown in the form of a coherent variation at longer time scales. The time series of MSC regions 1-5 do appear to decrease together after the mid-1970's, but coherent variations are not present as in Figure 4 (such as the rise and fall of stratiform clouds between 1990 and 2000 or the similar pattern in cumulus between 1995 and 2005). Further, a comparison of long-term variation at different frequencies (representing different time scales) in these time series did not suggest a large amount of coherence between regions. This does not completely exclude spurious variation from being the cause of the decrease, but the strong correlation of the interannual variations with SST, which is apparently increasing, grants *some* validity to the long-term MSC decline. Further, using multiple temperature datasets Deser et al. (2010) and Hansen et al. (2010) corroborate the SST trends for these five regions. They show increases in SST and surface temperature from 1900 through 2008 and 2009, respectively.

Linear fits to reanalysis data appear the most suspicious, as numerous studies (Bengtsson et al. 2004, Bromwich and Fogt 2004, Dee et al. 2010, Marshall and Harangozo 2000, Thorne and Vose 2010) show that while interannual variations are observable and compare well with other variables, long-term “trends” in reanalysis data are likely to be unreliable due to changing observing practices and

coverage.

The central Pacific is the only one of the six regions in which cloud cover correlates positively with SST. Figure 9 shows this as well as Figure 12, where cloud cover is correlated with the ENSO index. It is likely that in this region convection is driven by SST, and the warmer the sea surface, the stronger and deeper the convection, leading to greater and more persistent cloud cover at all levels. Correlations of the ENSO index with other cloud types show this, with positive correlations between ENSO and all cloud types except cumulus (indicating deeper convection with warmer SST). The linear fits to cloud cover in region 6, shown in table 3, suggest a warming sea surface, but long-term changes in the SST time series in this region are small, according to the IPCC (2007), possibly even negative as shown in Deser (2010). Part of the increase in cloud-cover is explained by the increase observed in the ENSO index over our period of record, which is roughly 0.1 per decade. To test this, a least-squares fit was made to the x-y scatter-plot between the ENSO index (x-axis) and cloud amounts (y-axis). The slope of this fit was then multiplied by the observed change in ENSO in order to see what the expected change produced by the increasing ENSO index may be. For the changes in total cloud cover, roughly one third of the increase was explained by ENSO, indicating that this slight increase in the ENSO index is only partly responsible for the observed cloud changes. A nearly identical result was obtained by Norris (2005) concerning an observed increase in upper-level clouds. This regression does not take into account the error in the fits, which makes any result quantitatively inexact.

The negative correlation between ENSO and total cloud cover seen in DJF over the equatorial western Pacific is not likely driven directly by changes in SST. Increased subsidence is a likely cause due to the shifting of convection to the central Pacific. Park and Leovy (2004) show that this negative correlation is the result of reduced northeasterly monsoon winds associated with a positive ENSO. Correlations of cloud types with ENSO support this, showing less precipitating, low stratiform, middle, and high level clouds during positive ENSO events. In the eastern equatorial Pacific the negative correlation between ENSO and total cloud cover during JJA and SON is driven by changes in low

stratiform clouds, particularly Sc, and is caused by changes in SST. Mitchell and Wallace (1992) showed that SST is at a minimum in this region between June and December due to the northward migration of the intertropical convergence zone. During a positive ENSO event this region of normally cool SST warms, reducing the SST gradient and decreasing static stability. Park and Leovy (2004) showed that this change in SST brings about a transition from stratiform to cumulus cloud cover. This is demonstrated in Figure 14 where correlations between ENSO and both stratiform and cumulus clouds are shown during JJA and SON.

Aside from SST, other factors certainly play a role in the variation of MSC. George and Wood (2010) shows that changing SLP, associated with changing circulation, plays a role in modulating MSC. Changing aerosol concentrations in the atmosphere could be a factor as well. Differing aerosol amounts could prolong or shorten the lifetime of clouds, and changes in aerosols are shown by Cermak et al. (2010). More thorough study of circulation and aerosol variation in our specified regions of MSC change may provide more insight.

A positive feedback between cloud cover and temperature in the NE Pacific was suggested by Clement et al. (2009). Our results are consistent with that suggestion but can extend it to other regions of persistent MSC decks, including regions offshore of the west coasts of South America, southern Africa, southern Europe, and Australia. The proposed mechanism for this feedback begins with warming SST's. Marine stratiform cloudiness is shown to be associated with cool SST and, as suggested by Norris and Leovy (1994), a reduction in cloud cover follows the warming sea surface. The loss of MSC allows more sunlight to reach the ocean surface thus warming the sea surface further. Observed changes in cloud-cover should be considered carefully, however, since spurious variation in the data set is still not fully understood.

7. Conclusion

The ocean is cloudier than the land, particularly in regards to low clouds. Over the ocean,

decadal-scale variations are present in the surface observed record of cloud cover for most cloud types. A test comparing the cloud record from ship reports to that from observations on islands in the central Pacific suggests that many of these long-term variations are spurious, particularly those that are coherent across many latitude zones. It is possible that a change over time in the fraction of nations contributing ship reports could be responsible for these spurious variations, however an exact cause is yet to be identified. In order to study variations in cloud cover as well as relationships between cloud cover and other variables we recommend accounting for this long-term variation. In the case of this paper a low-pass Butterworth filter is used to remove spurious variation from the time series for each cloud type.

Using adjusted data, anomalies of cloud amounts are shown to correlate with SST and LTS. A strong negative correlation is seen between low stratiform cloud cover and SST, while a positive correlation is seen between low stratiform cloud cover and LTS in regions of persistent MSC. This is an expected result, given previous work. Other factors such as sea level pressure and relative humidity also correlate with variations in low cloud cover. High clouds show a less substantial, but consistent, positive correlation with SST.

Given the subtle long-term variation in cloud cover shown on the global-scale, spurious variation makes finding trends on a large scale a perilous pursuit. Looking at smaller regions (adjusted for the long-term global variation), a possible increase in total cloud cover is observed in the central Pacific, while possible declines are seen in stratiform cloud cover in regions of persistent MSC. The decline in MSC is accompanied by an increase in SST between 1954 and 2008. Lower tropospheric stability and sea level pressure show long-term increases, apparently inconsistent with the changes in MSC and SST. An evaluation of previous works lends more confidence towards the SST changes, though in future work aerosol and circulation changes should also be taken into consideration. This decline in MSC and the warming of the sea surface, taken together with the negative correlation between MSC and SST, suggests a positive feedback to warming in regions of persistent MSC. In the

central Pacific, the the change in the ENSO index is not substantial enough to account for the observed cloud changes.

Acknowledgements:

The research was supported by NSF's Climate Dynamics Program and NOAA's Climate Change Data and Detection (CCDD) program, under NSF Grants ATM-0630428 and ATM-0630396. We thank Robert Wood, George Kiladis, and Mike Wallace for helpful discussion. Useful comments on the manuscript were provided by Joel Norris and two anonymous reviewers.

References

- Bajuk, L.J., and C.B. Leovy, 1998: Are there real interdecadal variations in marine low clouds? *J. Climate*, **11**, 2910-2921.
- Bengtsson, L., S. Hagemann, and K. I. Hodges, 2004: Can climate trends be calculated from reanalysis data? *J. Geophys. Res.*, **109**, D11111, doi: 10.1029/2004JD004536.
- Bony, S. and J.-L. Dufresne, 2005: Marine boundary clouds at the heart of tropical cloud feedback uncertainties in climate models. *Geophys. Res. Lett.* **32**, L20806, doi:10.1029/2005GL023851.
- Bromwich, D. H., and R. L. Fogt, 2004: Strong trends in the skill of the ERA-40 and NCEP/NCAR reanalyses in the high and middle latitudes of the southern hemisphere, 1958-2001. *J. Climate*, **17**, 4603-4619.
- Cermak, J., M. Wild, R. Knutti, M. I. Mishchenko, and A. K. Heidinger, 2010: Consistency of global satellite-derived aerosol and cloud data sets with recent brightening observations. *Geophys. Res. Lett.* **37**, L21704, doi: 10.1029/2010GL044632.
- Clement, A.C., R. Burgman, and J.R. Norris, 2009: Observational and model evidence for positive low-level cloud feedback. *Science*, **325**, 460-464. doi: 10.1126/science.1171255.
- Dee, D. P., E. Kallen, A. J. Simmons, and L. Haimberger, 2010: Comments on “Reanalysis suitable for characterizing long-term trends”. *Bull. Amer. Met. Soc.*, in press. Available online, doi:

10.1175/2010BAMS3070.1.

Deser, C., A. S. Phillips, and M. A. Alexander, 2010: Twentieth century tropical sea surface temperature trends revisited. *Geophys. Res. Lett.*, **37**, L10701, doi: 10.1029/2010GL043321.

Eastman, R., and S. G. Warren, 2010a: Interannual variations of Arctic cloud types in relation to sea ice. *J. Climate*. **23**, 4216-4232.

Eastman, R., and S. G. Warren, 2010b: Arctic cloud changes from surface and satellite observations. *J. Climate*. **23**, 4233-4242.

George, R. C. and R. Wood, 2010: Subseasonal variability of low cloud radiative properties over the southeast Pacific Ocean, *Atmos. Chem. Phys.*, **10**, 4047-4063, doi:10.5194/acp-10-4047-2010.

Hahn, C.J., S.G. Warren, and J. London, 1995: The effect of moonlight on observation of cloud cover at night, and application to cloud climatology. *J. Climate*, **8**, 1429-1446.

Hahn, C.J., and S.G. Warren, 1999 (Updated 2009): *Extended Edited Cloud Reports from Ships and Land Stations over the Globe, 1952-1996*. Numerical Data Package NDP-026C, Carbon Dioxide Information Analysis Center (CDIAC), Department of Energy, Oak Ridge, Tennessee (Documentation, 79 pages).

Hahn, C.J., and S.G. Warren, 2007 (Updated 2009): *A Gridded Climatology of Clouds over Land (1971-96) and Ocean (1954-97) from Surface Observations Worldwide*. Report NDP-026E, Carbon Dioxide Information Analysis Center, Oak Ridge, Tennessee, USA. 71pp.

<http://cdiac.ornl.gov/ftp/ndp026/>

Hamming, R. W., 1989: *Digital Filters*. Prentice Hall, 284pp.

Hansen, J., R. Ruedy, M. Sato, and K. Lo, 2010: Global surface temperature change. *Rev. Geophys.*, in press.

IPCC, 2007: *Climate Change 2007: The Physical Science Basis. Contribution of Working Group I to the Fourth Assessment Report of the Intergovernmental Panel on Climate Change* [Solomon, S., D. Qin, M. Manning, Z. Chen, M. Marquis, K.B. Averyt, M. Tignor and H.L. Miller (Eds.)]. Cambridge University Press, Cambridge, United Kingdom and New York, NY, USA, 996 pp.

Kalnay, E., M. Kanamitsu, R. Kistler, W. Collins, D. Deaven, L. Gandin, M. Iredell, S. Saha, G. White, J. Woollen, Y. Zhu, M. Chelliah, W. Ebisuzaki, W. Higgins, J. Janowiak, K. C. Mo, C. Ropelewski, J. Wang, A. Leetmaa, R. Reynolds, R. Jenne, and D. Joseph, 1996: The NCEP/NCAR 40 year reanalysis project, *Bull. Amer. Meteor. Soc.*, **77**, 437-470.

Kato, S., 2009: Interannual variability of the global radiation budget. *J. Climate*, **22**, 4893-4907.

Klein, S.A., and D.L. Hartmann, 1993: The seasonal cycle of low stratiform clouds. *J. Climate*, **6**, 1587-1606.

Lanzante, J.R., 1996: Resistant, robust and non-parametric techniques for the analysis of climate data: Theory and examples, including applications to historical radiosonde station data. *Int. J. Climatol.*, **16**, 1197-1226.

Marshall, J. G., and S. A. Harangozo, 2000: An appraisal of NCEP/NCAR reanalysis MSLP data viability for climate studies in the South Pacific. *Geophys. Res. Lett.*, **27**, 3057-3060, doi: 10.1029/2000GL011363.

Mendenhall, W., R. L. Scheaffer, and D. D. Wackerly, 1981: *Mathematical Statistics with Applications*. 2nd ed. Duxbury Press, 686pp.

Meyers, S.D., J.J. O'Brien, and E. Thelin, 1999: Reconstruction of monthly SST in the tropical Pacific Ocean during 1868-1993 using adaptive climate basis functions. *Mon. Wea. Rev.*, **127**, 1599-1612.

Mitchell, T. P., and J. M. Wallace, 1992: The annual cycle in equatorial convection and sea surface temperature. *J. Climate*, **5**, 1140-1156

Norris, J.R., and C.B. Leovy, 1994: Interannual variability in stratiform cloudiness and sea surface temperature. *J. Climate*, **7**, 1915-1925.

Norris, J.R., 1999: On trends and possible artifacts in global ocean cloud cover between 1952 and 1995. *J. Climate*, **12**, 1864-1870.

Norris, J.R., 2000: What can cloud observations tell us about climate variability? *Space Sci. Rev.* **94**, 375-380.

Norris, J. R., 2002: Evidence for globally decreasing subtropical Stratocumulus since 1952. *Proceedings of the 2002 Fall AGU meeting*.

<http://meteora.ucsd.edu/~jnorris/presentations/AGU2002.pdf>

Norris, J.R., 2005: Trends in upper-level cloud cover and surface divergence over the tropical Indo-Pacific Ocean between 1952 and 1997. *J. Geophys. Res.*, **110**, D21110, doi:10.1029/2005JD006183.

Park, S. and C. B. Leovy, 2004: Marine low-cloud anomalies associated with ENSO. *J. Climate*, **17**, 3448-3469.

Press, W.H., S.A. Teukolsky, W.T. Vetterling, and B.P. Flannery, 2002: *Numerical Recipes in C: The Art of Scientific Computing*. 2nd ed. Cambridge University Press, 994 pp.

Randall, D.A., J.A. Coakley Jr., C.W. Fairall, A. Kropfli, and D.H. Lenschow, 1984: Outlook for research on subtropical marine stratiform clouds. *Bull. Amer. Meteor. Soc.*, **65**, 1290-1301.

Rayner, N. A., D. E. Parker, E. B. Horton, C. K. Folland, L. V. Alexander, D. P. Rowell, E. C. Kent, and A. Kaplan, 2003: Global analyses of sea surface temperature, sea ice, and night marine air temperature since the late nineteenth century. *J. Geophys. Res.* **108**, No. D14, 4407
10.1029/2002JD002670

Thorne, P. W., and R. S. Vose, 2010: Reanalysis suitable for long-term trends: Are they really achievable? *Bull. Amer. Met. Soc.*, **91**, 353-361.

Trenberth, K. E., and J. T. Fasullo, 2009: Global warming due to increasing absorbed solar radiation. *Geophys. Res. Lett.* **36**, L07706, doi: 10.1029/2009GL037527.

WMO, 1956: *International Cloud Atlas*. World Meteorological Organization, 62pp. plus 72 plates.

WMO, 1974: *Manual on Codes*. Vol. 1. World Meteorological Organization Publication 306, 348 pp.

Warren, S. G., C. J. Hahn, and J. London, 1985: Simultaneous occurrence of different cloud types.

Journal of Climate and Applied Meteorology, **24**, 7, 658-667.

Warren, S. G., C. J. Hahn, J. London, R. M. Chervin, and R. L. Jenne, 1988: Global distribution of total cloud cover and cloud type amounts over the ocean. NCAR Tech. Note TN-317+STR, 212pp.

Warren, S. G., and C. J. Hahn, 2002: Cloud climatology. *Encyclopedia of Atmospheric Sciences*, 476-483. Oxford University Press.

Warren, S. G., R. M. Eastman, and C.J. Hahn, 2007: A survey of changes in cloud cover and cloud types over land from surface observations, 1971-1996. *J. Climate*, **20**, 717-738.

Wood, R., and D.L. Hartmann, 2006: Spatial variability of liquid water path in marine low clouds: The importance of mesoscale cellular convection. *J. Climate*, **19**, 1748-1764.

Woodruff, S.D., R.J. Slutz, R.L. Jenne, and P.M. Steurer, 1987: A comprehensive ocean atmosphere data set. *Bull. Amer. Meteor. Soc.*, **68**, 1239-1250.

Woodruff, S.D., H.F. Diaz, J.D. Elms, and S.J. Worley, 1998: COADS Release 2 data and metadata enhancements for improvements of marine surface flux fields. *Phys. Chem. Earth*, **23**, 517-526.

Worley, S.J., S.D. Woodruff, R.W. Reynolds, S.J. Lubker, and N. Lott, 2005: ICOADS Release 2.1 data and products. *Int. J. Climatol.*, **25**, 823-842.

Wyant, M.C., C.S. Bretherton, H.A. Rand, and D.E. Stevens, 1997: Numerical simulations and a conceptual model of the stratocumulus to trade cumulus transition. *J. Atmos. Sci.* **54**, 169-192.

Wylie, D., D. L. Jackson, W. P. Menzel, and J. J. Bates, 2005: Trends in global cloud cover in two decades of HIRS observations. *J. Climate*. **18**, 3021-3031.

Figure 1. Number of ship observations per year used to form the cloud climatology.

Figure 2. Seasonal values of average total cloud cover for day and night separately, for each of six selected grid boxes from 1954 to 2008. Day is defined as 0600 - 1800 local time. For the Indonesian box (frames k, l) only the oceanic part of the box is represented because only observations from ships were used.

Figure 3. Scatter plots of day versus night cloud cover anomalies, DJF 1954-2008. Each point is one season in one grid box. The correlation value (r^2) is also given.

Figure 4. Annual average daytime cloud cover anomalies for total, low, middle, and high clouds as well as low cloud types St, Sc, St+Sc and Cu. Global average anomalies are plotted in bold and 10° zonal anomalies (scaled to zonal average cloud amount, using eq. 1) are shown in gray. Coherent variations are seen across most latitude zones for most types.

Figure 5. The region where island-observed clouds are compared with ship-observed clouds is outlined in black.

Figure 6. Butterworth-filtered and unaltered time series of daytime cloud-amount anomalies observed from islands (gray) and ships (black) in the central Pacific Ocean. Four points per year are plotted.

Figure 7. Scatter plots of residuals (the filtered time series subtracted from the anomaly time series) from Figure 6. Linear correlation coefficient and significance shown on bottom right of each panel.

Figure 8. Global time series of seasonal, daytime total cloud cover anomalies computed for (a) land and (b) ocean areas. Spurious variation over the ocean has not been corrected for in this figure. Over land, seasonal anomalies were obtained from individual weather stations, relative to the long-term mean for that station during that season. Station anomalies were then averaged within each $10^\circ \times 10^\circ$ grid box; then all grid boxes were averaged, weighted by their relative sizes and land fractions. Over the ocean, seasonal anomalies for each season were computed for each $10^\circ \times 10^\circ$ grid box. Seasonal anomalies in each box were then averaged to form global seasonal anomalies, weighted by relative box area and ocean fraction.

Figure 9. Correlations between SST (UK Met Office HadISST1) time series and daytime (a) total cloud cover, (b) low cloud amount, and (c) high cloud amount. A low-pass Butterworth filter is used to remove long-term variation from both time series in each grid box before correlation. Correlations are shown as dots, with larger dots representing larger magnitude correlations, white dots representing positive correlations and black dots representing negative. Cloud amount and SST anomalies are seasonal anomalies relative to long-term seasonal means. These plots were also done using surface air temperature and lower tropospheric stability (LTS) from the NCEP/NCAR reanalysis, producing nearly identical results (reversed relationship for LTS). Dots surrounded by a gray ring indicate significance at the 99% level.

Figure 10. Scatter plots of daytime stratiform (black) and cumulus (gray) cloud amount anomalies versus SST for region 5 in Figure 11, off the SW coast of Africa. Data are plotted for all seasons from 1954 through 2008. Long term variation is removed from both time series using a low-pass Butterworth filter. Best-fit lines are calculated using a least squares method taking error in both axes into account.

Figure 11. Regions (1-5) where MSC and SST correlate negatively. Region (6) where all cloud types but cumulus correlate positively with SST.

Figure 12. Linear correlations between the seasonal average ENSO index and daytime total cloud cover anomalies. Before computing the correlations, long term variation was removed from the time series in each box using a low-pass Butterworth filter. Dots are plotted using the same scheme as Figure 9. Dots surrounded by a gray ring indicate significance at the 99% level.

Figure 13. Time series of daytime MSC and SST in regions 1-6 defined in Figure 11. All values in the time series represent the regional, annual mean value, weighted by relative box and ocean areas. Long-term globally coherent variation is approximated using a low-pass Butterworth filter on the global MSC time series, scaled to the regional mean MSC amount, then subtracted from regional time series.

Figure 14. Linear correlations between the seasonal average ENSO index and daytime (a) stratiform cloud cover anomalies in JJA, (b) stratiform cloud cover anomalies in SON, (c) cumulus cloud cover anomalies in JJA, and (d) cumulus cloud cover anomalies in SON. Before computing the correlations, long-term variation is removed from the time series in each box using a low-pass Butterworth filter. Dots are plotted using the same scheme as Figures 9 and 12. Dots surrounded by a gray ring indicate significance at the 99% level.

Table 1. Global average cloud-type amounts and heights from surface observations. The cloud "amount" is the average percent of the sky covered. The amounts of all the cloud types add up to more than the total cloud cover because of overlap. Land values are for 1971-1996; ocean values are for 1954-2008. This table is an update to Table 2 of Warren et al. (2007).

Cloud Type	Annual Average Amount (%)		Base Height (meters above surface)	
	Land	Ocean	Land	Ocean
Fog	1	1	0	0
Stratus (St)	5	13	500	400
Stratocumulus (Sc)	12	22	1000	600
Cumulus (Cu)	5	13	1100	600
Cumulonimbus (Cb)	4	6	1000	500
Nimbostratus (Ns)	5	5		
Altostratus (As)	4	6		
Alto cumulus (Ac)	17	18		
High (ciriform)	22	12		
Total cloud cover	54	68		
Clear sky (frequency)	22	3		

Table 2. Correlation coefficients between Marine Stratiform Clouds (MSC), Cumulus clouds, sea surface temperature (SST), lower tropospheric stability (LTS; $\Theta_{850} - \Theta_{1000}$), surface relative humidity (RH), and sea-level pressure (SLP) for regions 1-6 in Figure 14. Correlations over 0.25 are significant at the 99% level.

Region 1						
	MSC	Cumulus	SST	LTS	RH	SLP
MSC	1.00	-0.50	-0.44	0.22	0.12	-0.06
Cumulus		1.00	0.24	-0.13	0.06	0.05
SST			1.00	-0.17	-0.02	-0.05
LTS				1.00	0.41	0.10
RH					1.00	-0.04
SLP						1.00
Region 2						
	MSC	Cumulus	SST	LTS	RH	SLP
MSC	1.00	-0.67	-0.54	0.49	0.37	0.42
Cumulus		1.00	0.26	-0.38	-0.30	-0.24
SST			1.00	-0.42	-0.09	-0.30
LTS				1.00	0.50	0.54
RH					1.00	0.16
SLP						1.00
Region 3						
	MSC	Cumulus	SST	LTS	RH	SLP
MSC	1.00	-0.53	-0.45	0.40	0.10	0.18
Cumulus		1.00	0.49	-0.22	-0.15	-0.26
SST			1.00	-0.33	-0.24	-0.65
LTS				1.00	0.25	0.14
RH					1.00	0.20
SLP						1.00
Region 4						
	MSC	Cumulus	SST	LTS	RH	SLP
MSC	1.00	-0.70	-0.49	0.51	0.30	0.26
Cumulus		1.00	0.25	-0.63	-0.42	-0.17
SST			1.00	-0.03	0.07	0.12
LTS				1.00	0.36	0.55
RH					1.00	-0.10
SLP						1.00
Region 5						
	MSC	Cumulus	SST	LTS	RH	SLP
MSC	1.00	-0.70	-0.57	0.57	0.32	0.41
Cumulus		1.00	0.43	-0.35	-0.19	-0.27
SST			1.00	-0.36	-0.41	-0.56
LTS				1.00	0.23	0.32
RH					1.00	0.25
SLP						1.00
Region 6						
	MSC	Cumulus	SST	LTS	RH	SLP
MSC	1.00	-0.56	0.46	0.23	0.26	-0.35
Cumulus		1.00	-0.25	-0.11	-0.24	0.19
SST			1.00	0.16	0.02	-0.62
LTS				1.00	0.40	-0.17
RH					1.00	-0.02
SLP						1.00

Table 3. Linear fits (in %/Decade) of time series of Marine Stratiform Clouds (MSC), Cumulus clouds, sea surface temperature (SST), lower tropospheric stability (LTS), surface relative humidity (RH) and sea level pressure for regions 1-6 in Figure 14. Time series span from 1954 through 2008.

Region	MSC	Cumulus	SST	LTS	RH	SLP
1	-0.56	-0.27	0.13	0.25	0.27	0.15
2	-0.68	0.38	0.04	0.13	0.17	-0.04
3	-0.98	0.18	0.07	0.21	0.23	0.05
4	-0.31	0.14	0.10	0.10	-0.11	0.17
5	-1.15	0.04	0.10	0.18	0.13	0.12
6	0.84	-0.03	0.08	0.14	0.09	0.12

(% / Decade) (% / Decade) (K / Decade) (K / Decade) (% / Decade) (hPa / Decade)

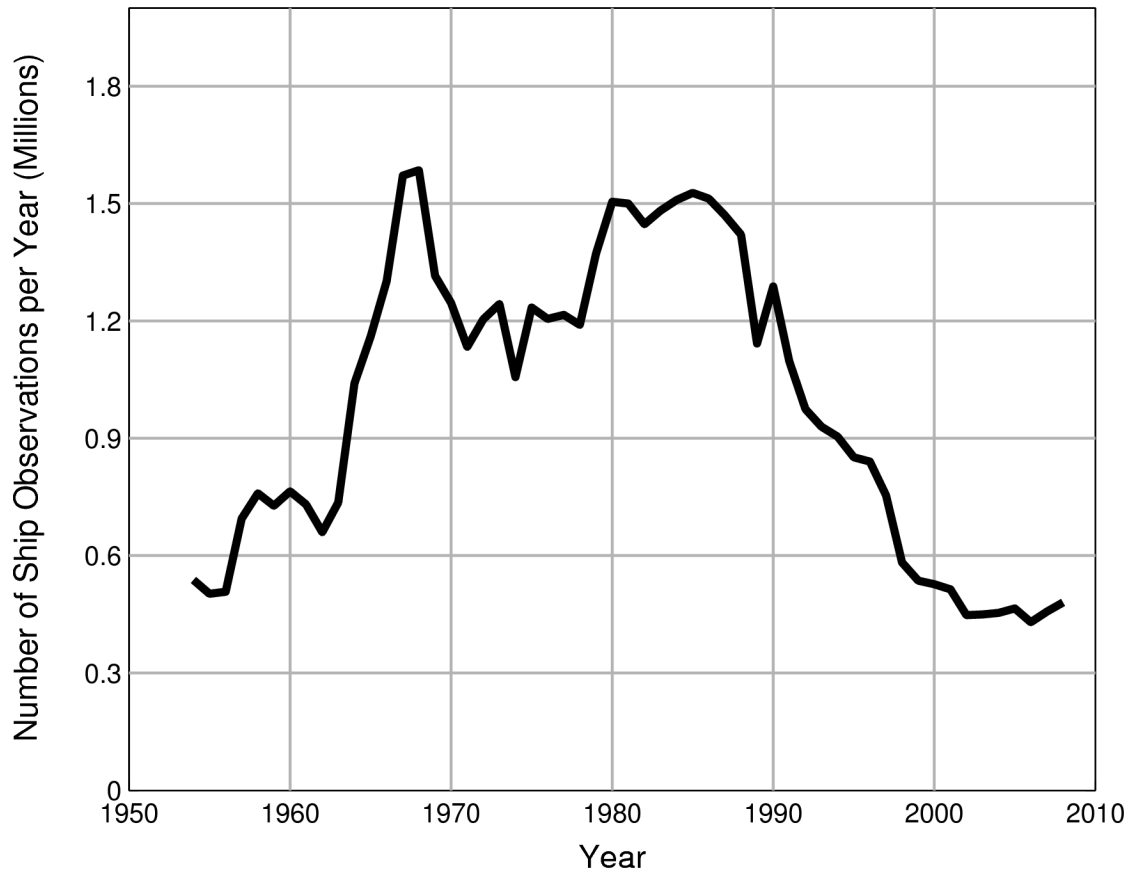


Figure 1. Number of ship observations per year used to form the cloud climatology.

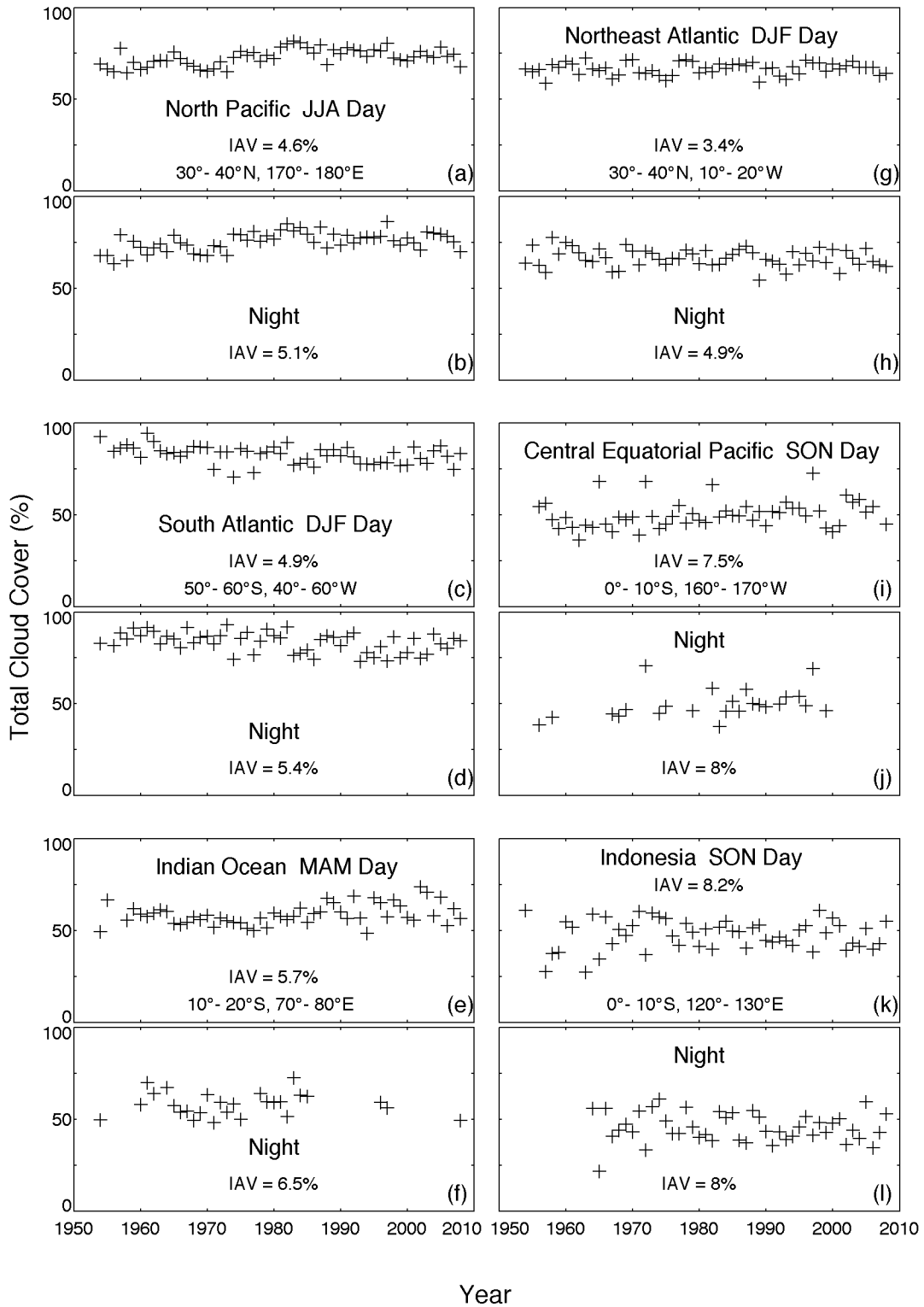


Figure 2. Seasonal values of average total cloud cover for day and night separately, for each of six selected grid boxes from 1954 to 2008. Day is defined as 0600 - 1800 local time. For the Indonesian box (frames k,l) only the oceanic part of the box is represented because only observations from ships were used.

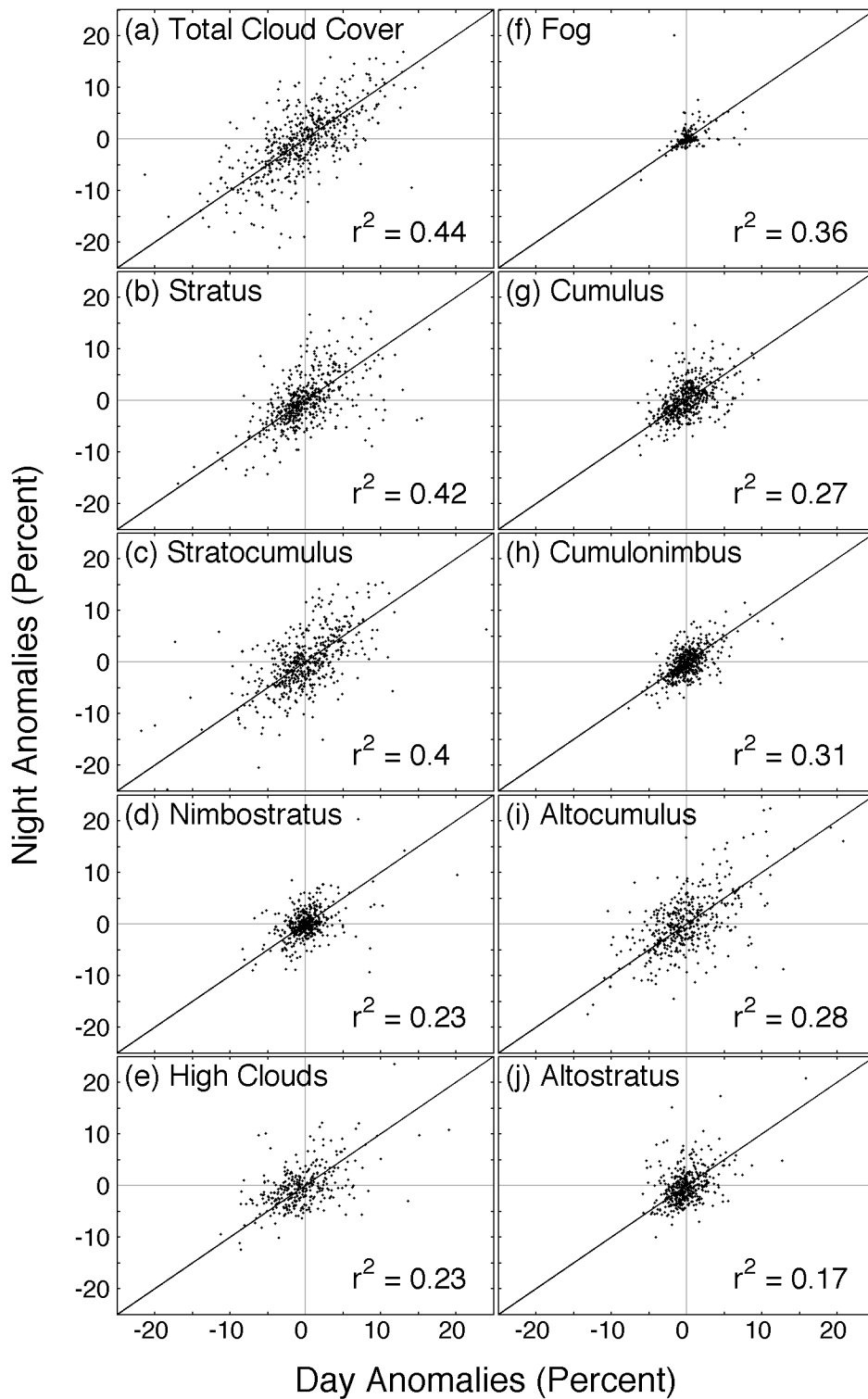


Figure 3. Scatter plots of day versus night cloud cover anomalies, DJF 1954-2008. Each point is one season in one grid box. The correlation value (r^2) is also given.

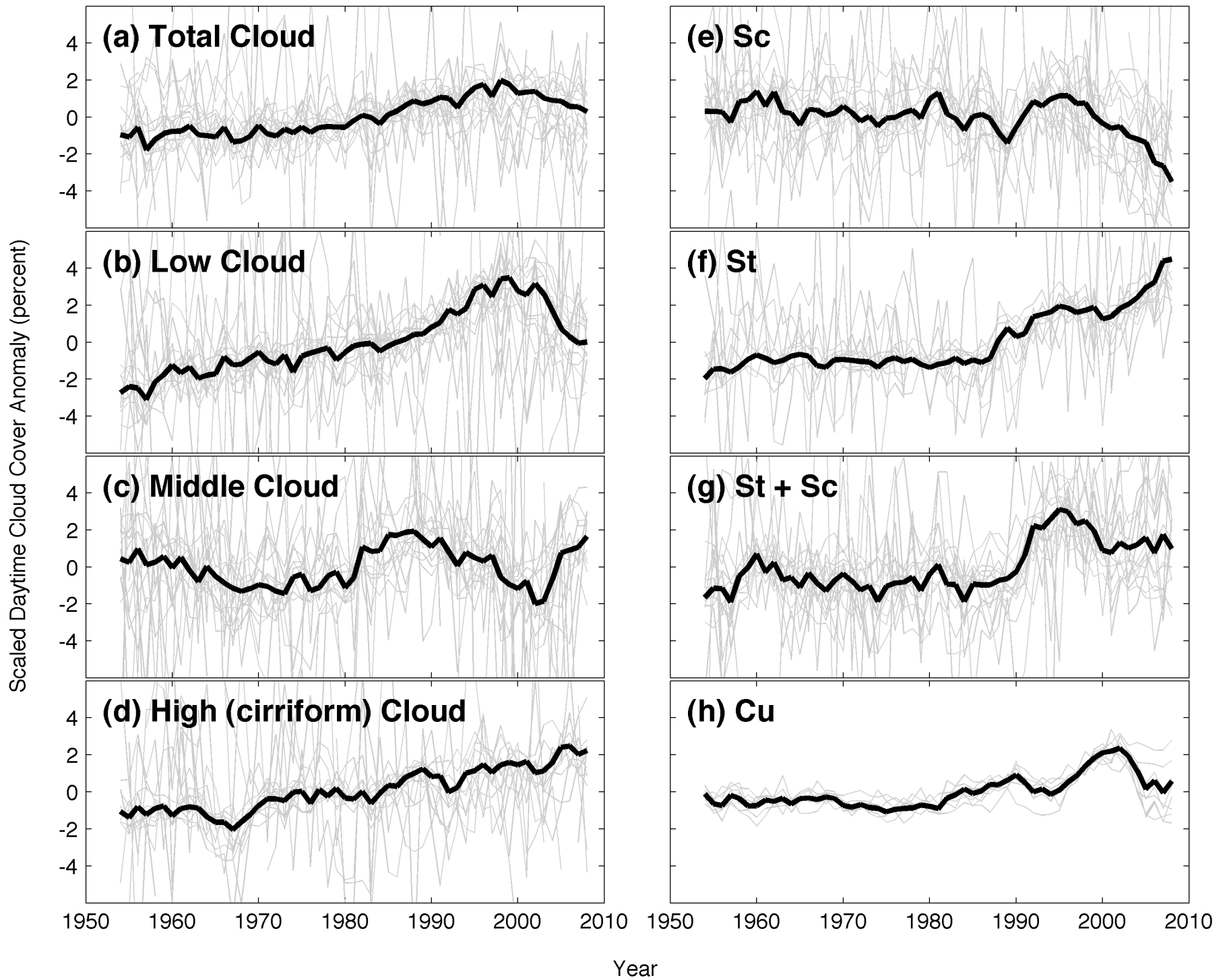


Figure 4. Annual average daytime cloud cover anomalies for total, low, middle, and high clouds as well as low cloud types St, Sc, St+Sc and Cu. Global average anomalies are plotted in bold and 10° zonal anomalies (scaled to zonal average cloud amount, using eq. 1) are shown in gray. Coherent variations are seen across most latitude zones for most types.

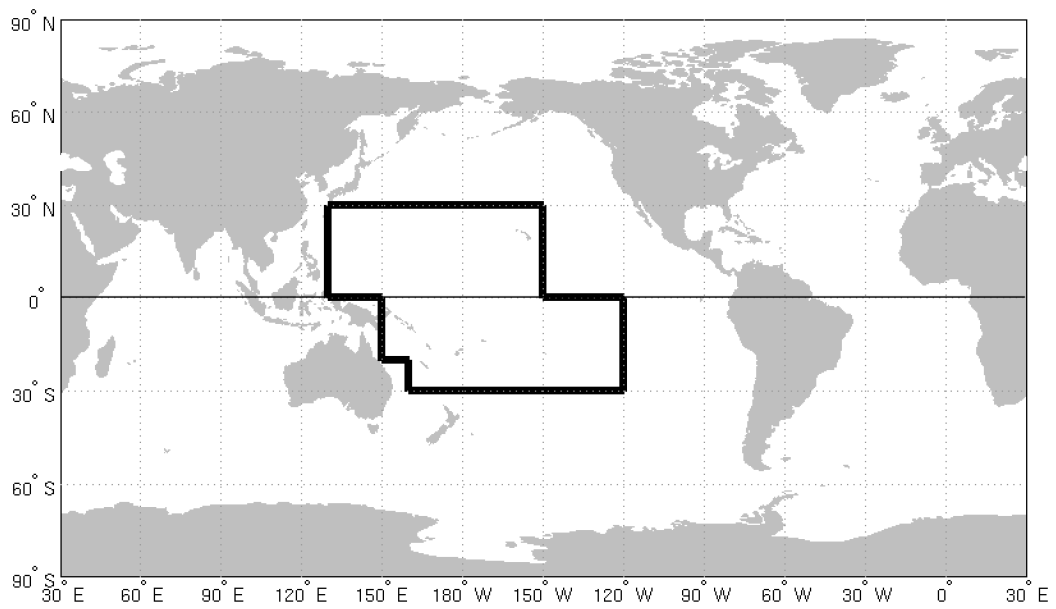


Figure 5. The region where island-observed clouds are compared with ship-observed clouds is outlined in black.

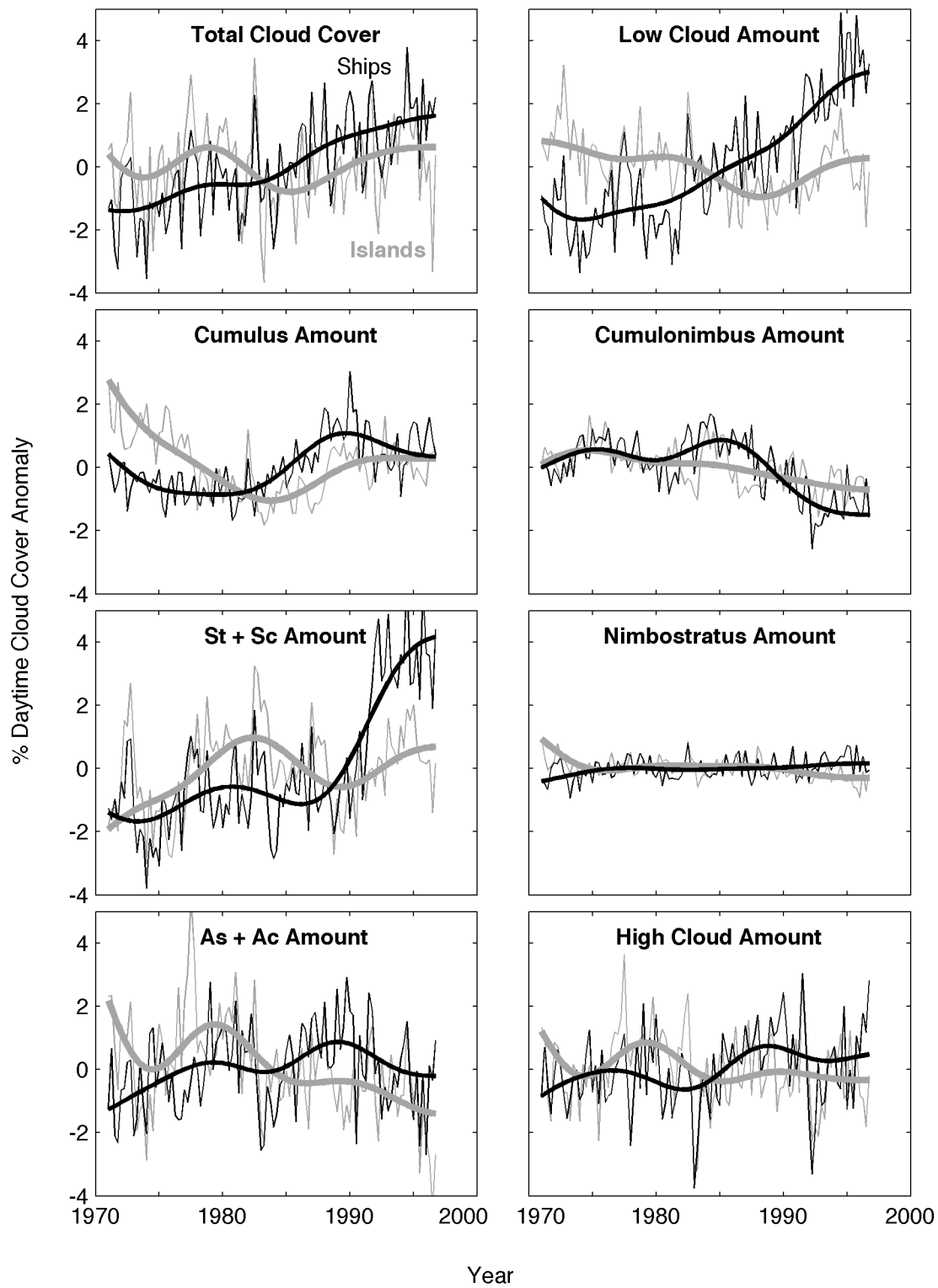


Figure 6. Butterworth-filtered and unaltered time series of daytime cloud-amount anomalies observed from islands (gray) and ships (black) in the central Pacific Ocean. Four points per year are plotted.

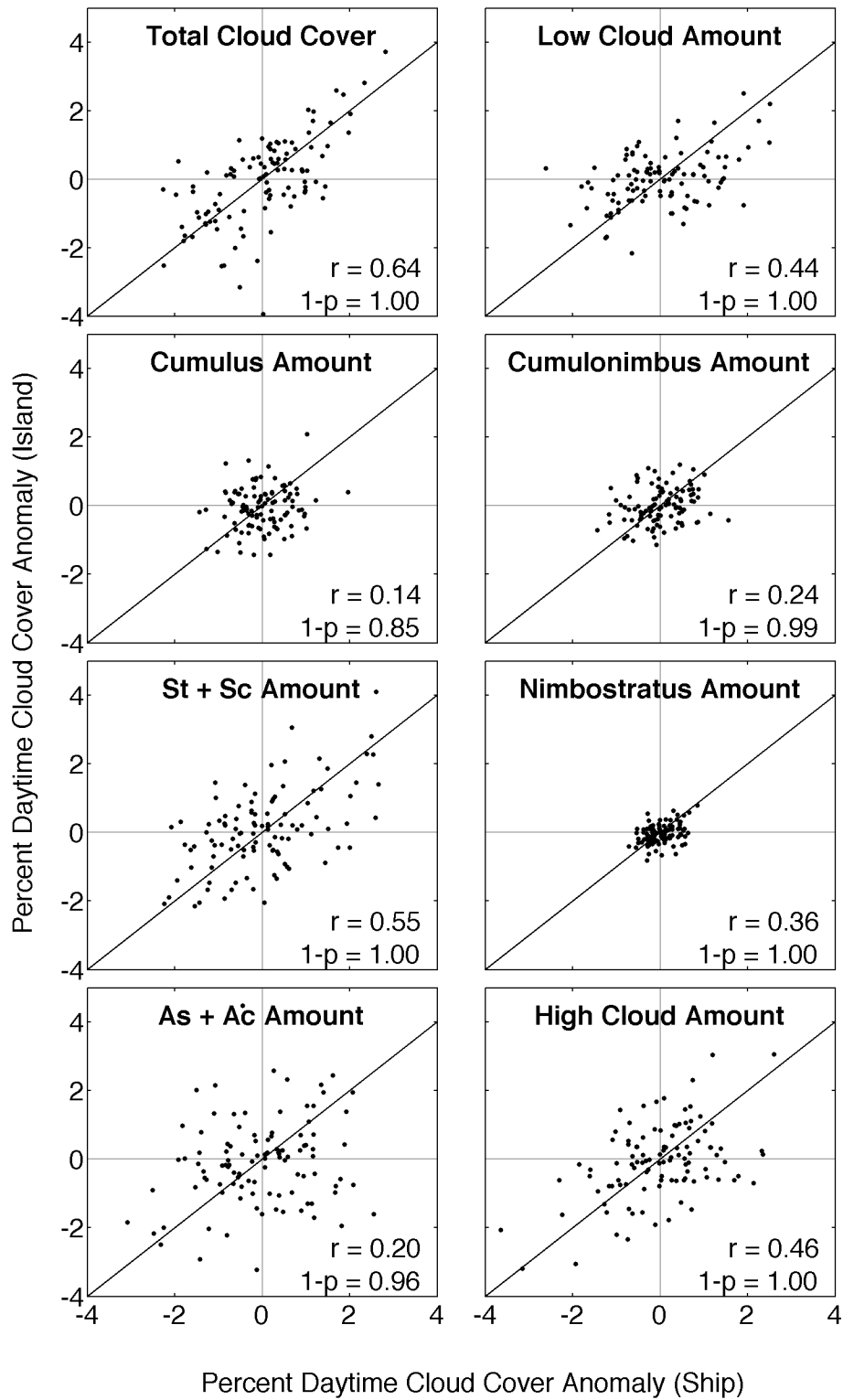


Figure 7. Scatter plots of residuals (the filtered time series subtracted from the anomaly time series) from Figure 6. Linear correlation coefficient and significance shown on bottom right of each panel.

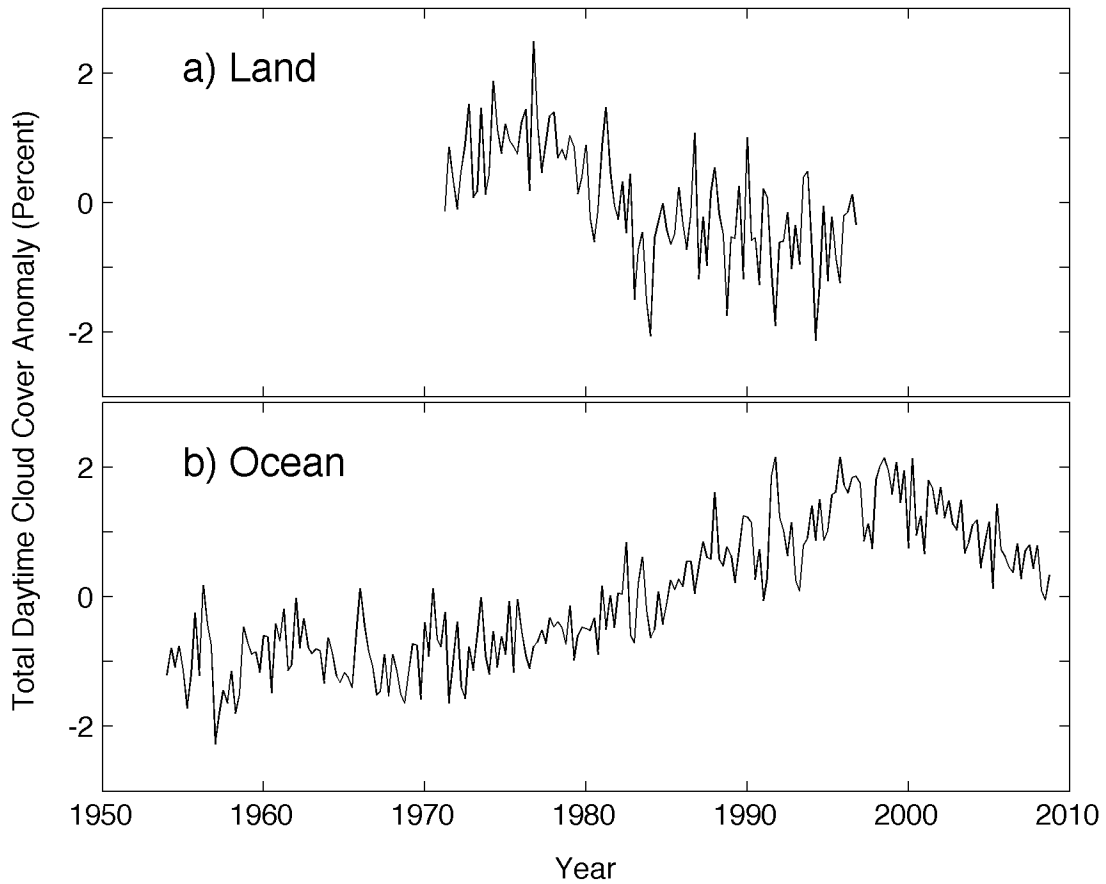


Figure 8. Global time series of seasonal, daytime total cloud cover anomalies computed for (a) land and (b) ocean areas. Spurious variation over the ocean has not been corrected for in this figure. Over land, seasonal anomalies were obtained from individual weather stations, relative to the long-term mean for that station during that season. Station anomalies were then averaged within each $10^\circ \times 10^\circ$ grid box; then all grid boxes were averaged, weighted by their relative sizes and land fractions. Over the ocean, seasonal anomalies for each season were computed for each $10^\circ \times 10^\circ$ grid box. Seasonal anomalies in each box were then averaged to form global seasonal anomalies, weighted by relative box area and ocean fraction.

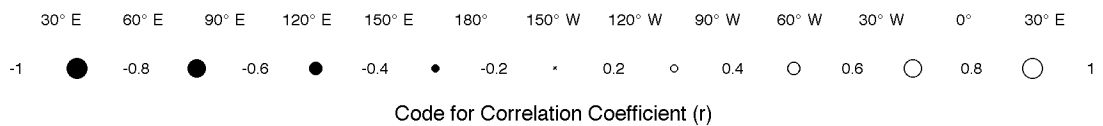
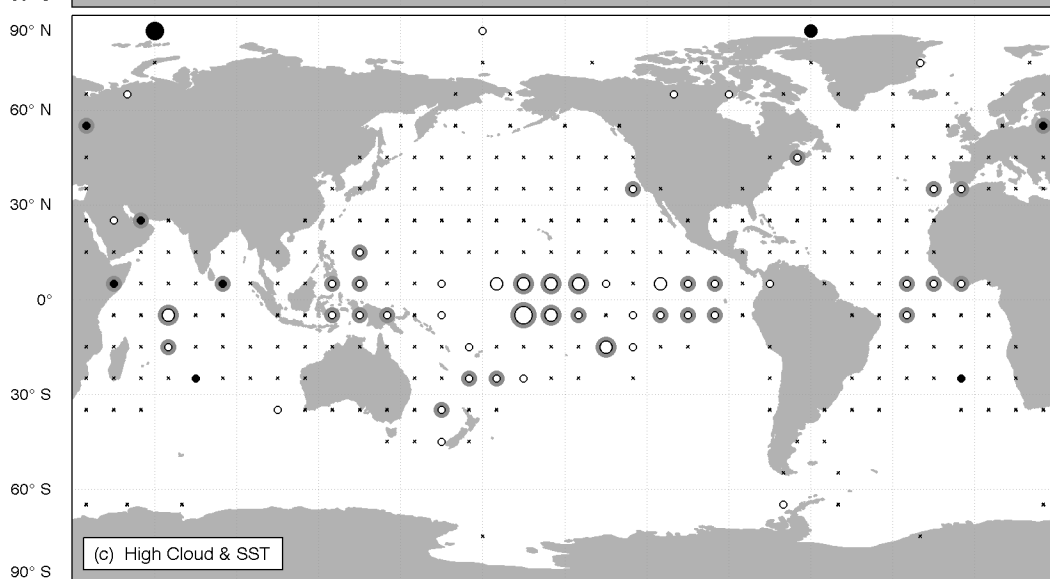
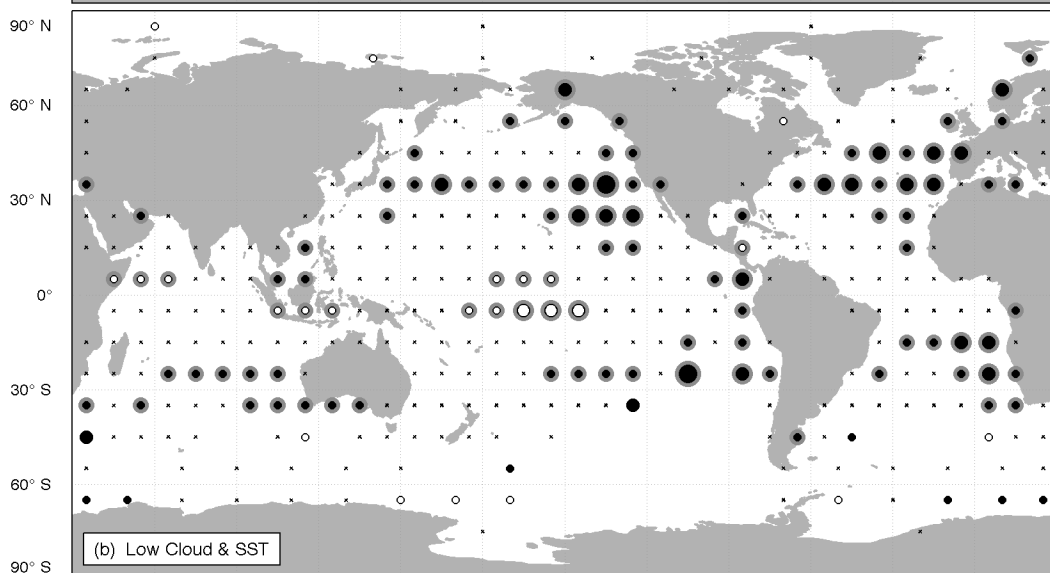
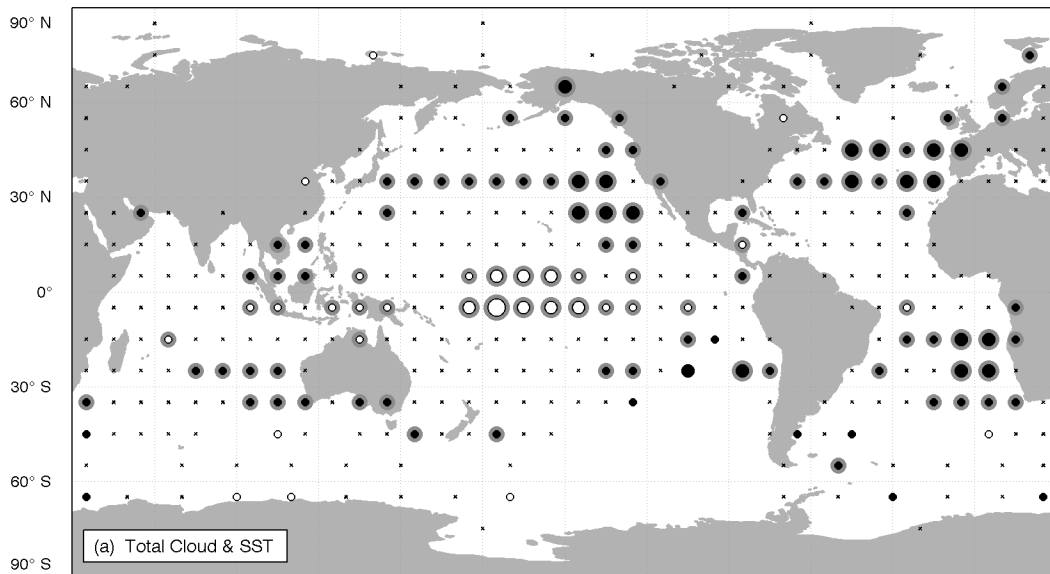


Figure 9. Correlations between SST (UK Met Office HadISST1) time series and daytime (a) total cloud cover, (b) low cloud amount, and (c) high cloud amount. A low-pass Butterworth filter is used to remove long-term variation from both time series in each grid box before correlation. Correlations are shown as dots, with larger dots representing larger magnitude correlations, white dots representing positive correlations and black dots representing negative. Cloud amount and SST anomalies are seasonal anomalies relative to long-term seasonal means. These plots were also done using surface air temperature and lower tropospheric stability (LTS) from the NCEP/NCAR reanalysis, producing nearly identical results (reversed relationship for LTS). Dots surrounded by a gray ring indicate significance at the 99% level.

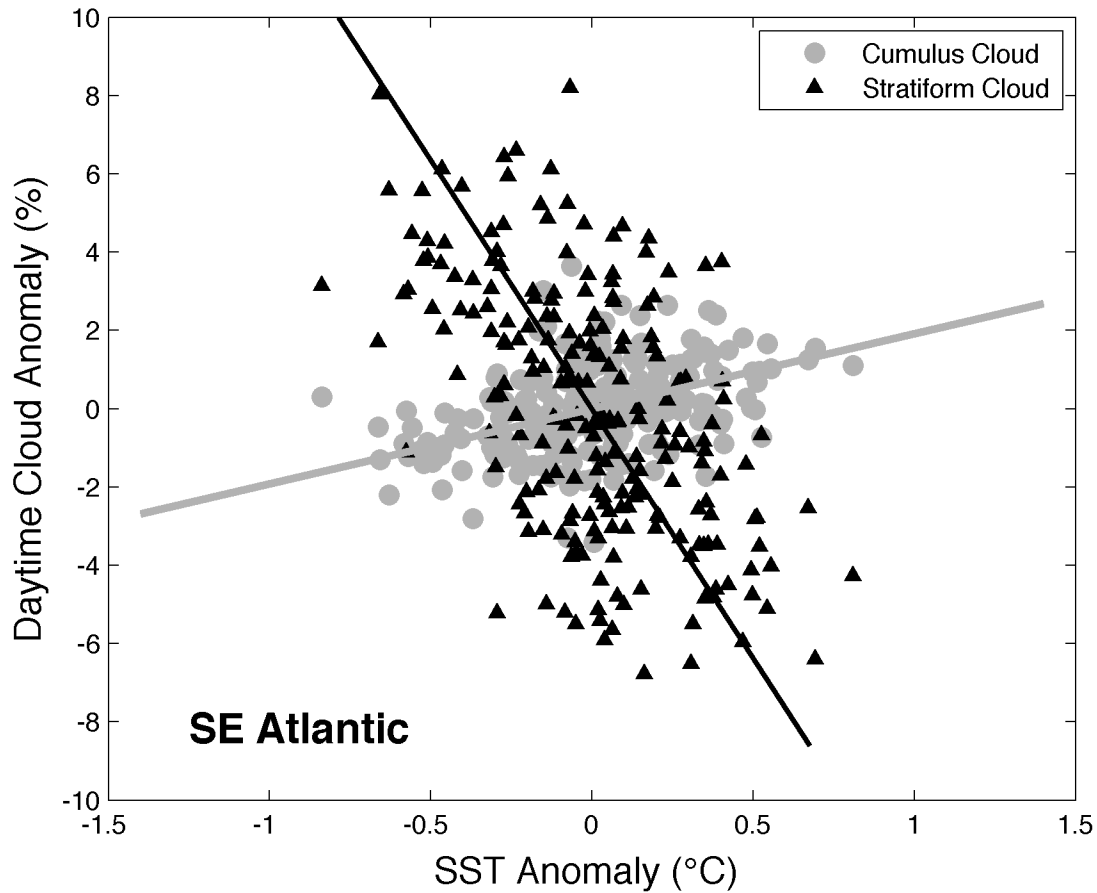


Figure 10. Scatter plots of daytime stratiform (black) and cumulus (gray) cloud amount anomalies versus SST for region 5 in Figure 11, off the SW coast of Africa. Data are plotted for all seasons from 1954 through 2008. Long term variation is removed from both time series using a low-pass Butterworth filter. Best-fit lines are calculated using a least squares method taking error in both axes into account.

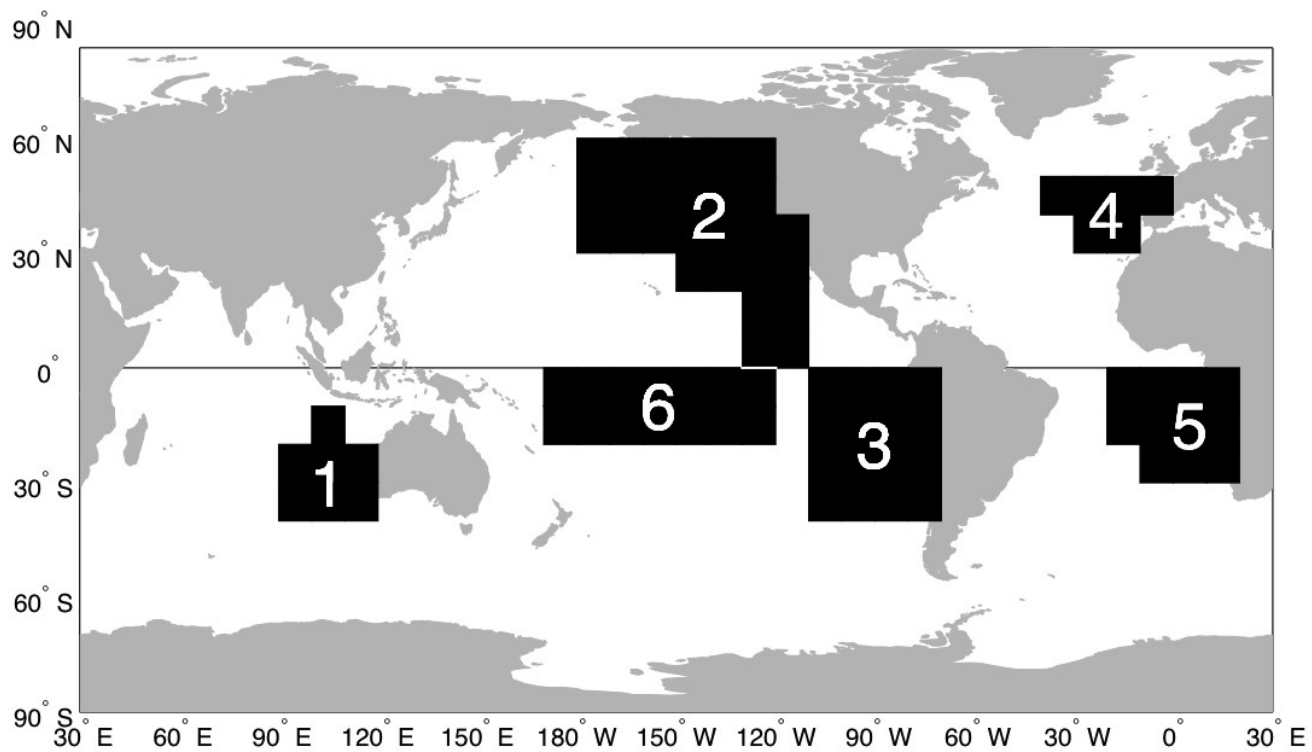


Figure 11. Regions (1-5) where MSC and SST correlate negatively. Region (6) where all cloud types but cumulus correlate positively with SST.

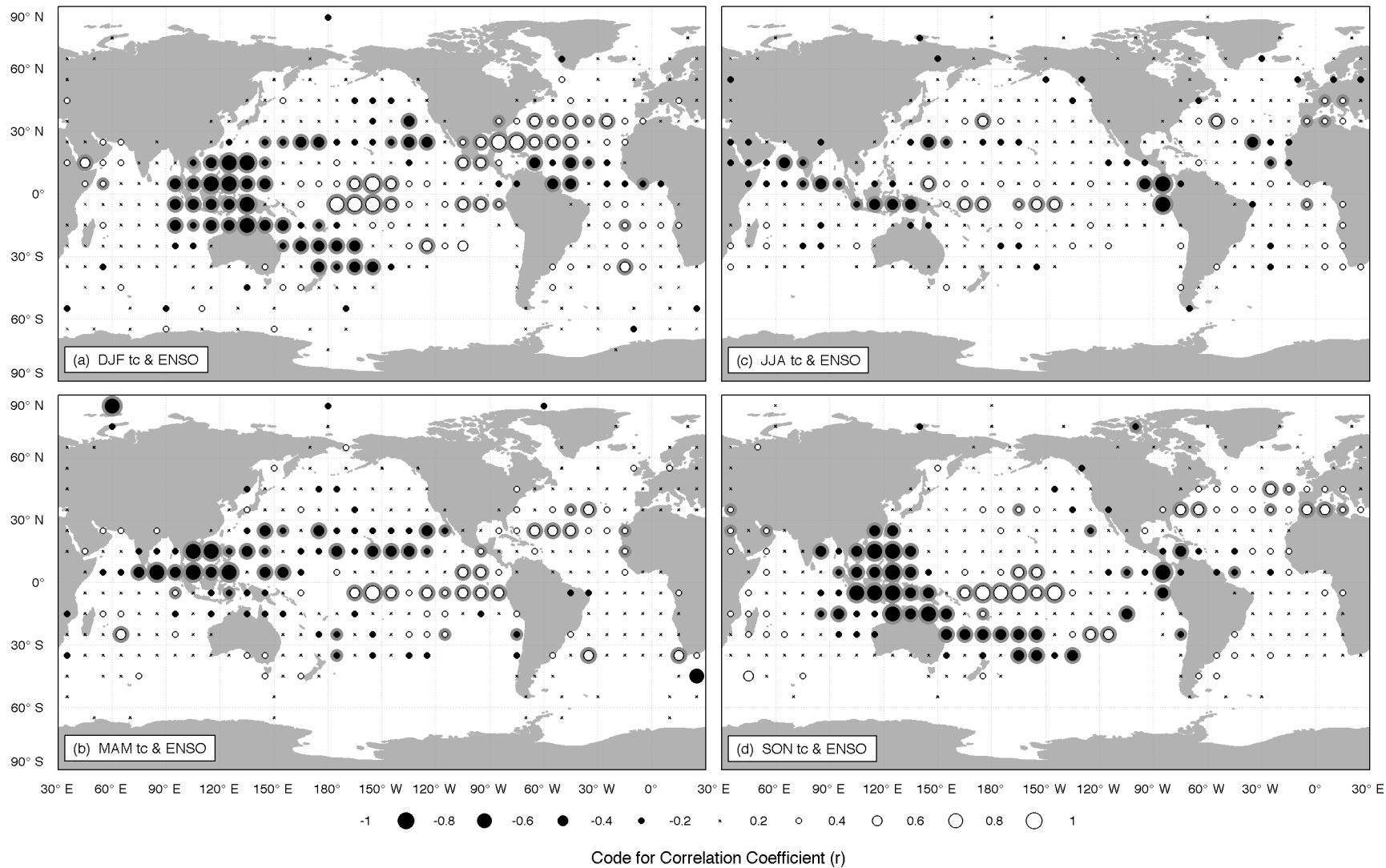


Figure 12. Linear correlations between the seasonal average ENSO index and daytime total cloud cover anomalies. Before computing the correlations, long term variation was removed from the time series in each box using a low-pass Butterworth filter. Dots are plotted using the same scheme as Figure 9. Dots surrounded by a gray ring indicate significance at the 99% level.

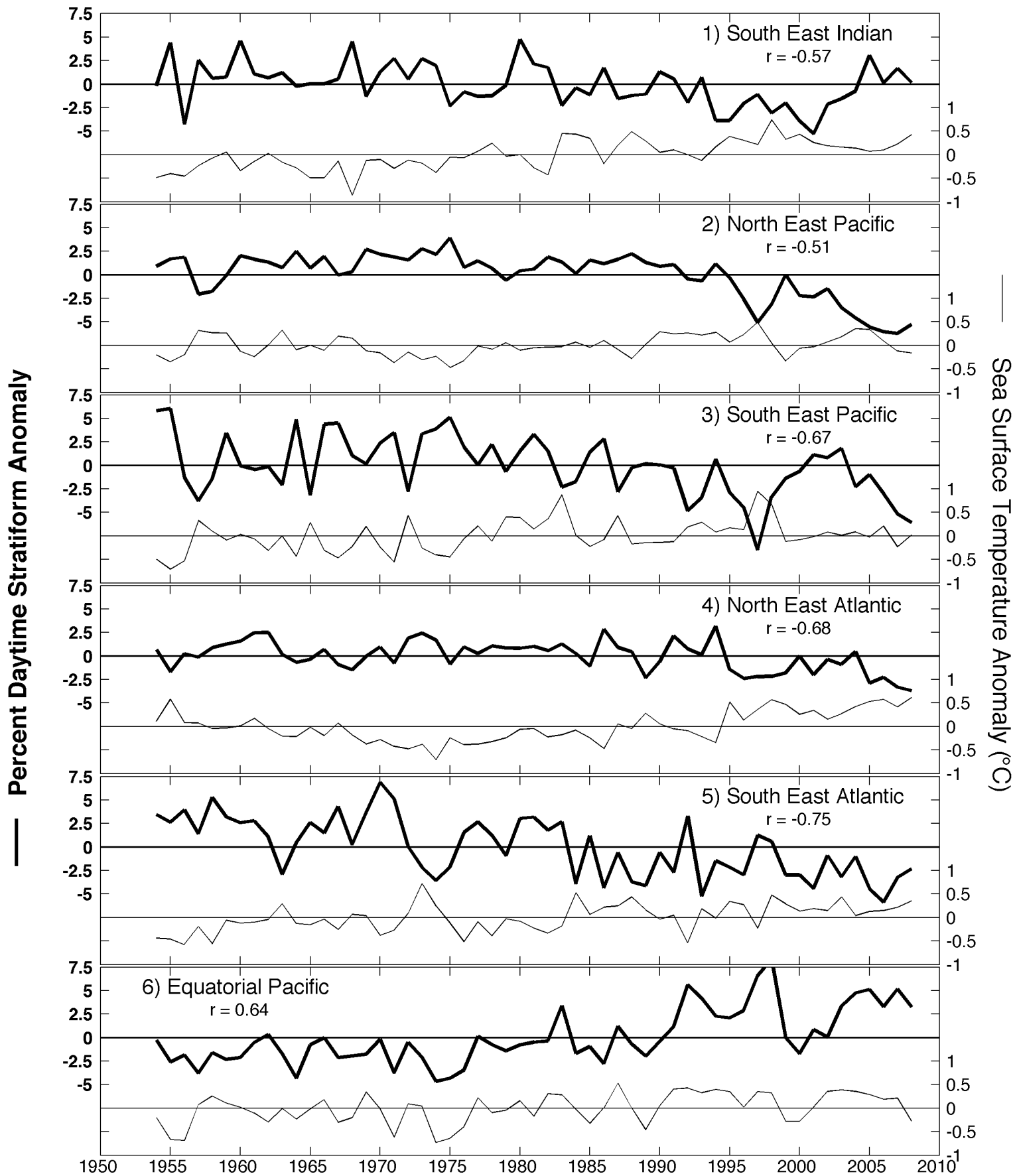


Figure 13. Time series of daytime MSC and SST in regions 1-6 defined in Figure 11. All values in the time series represent the regional, annual mean value, weighted by relative box and ocean areas. Long-term globally coherent variation is approximated using a low-pass Butterworth filter on the global MSC time series, scaled to the regional mean MSC amount, then subtracted from regional time series.

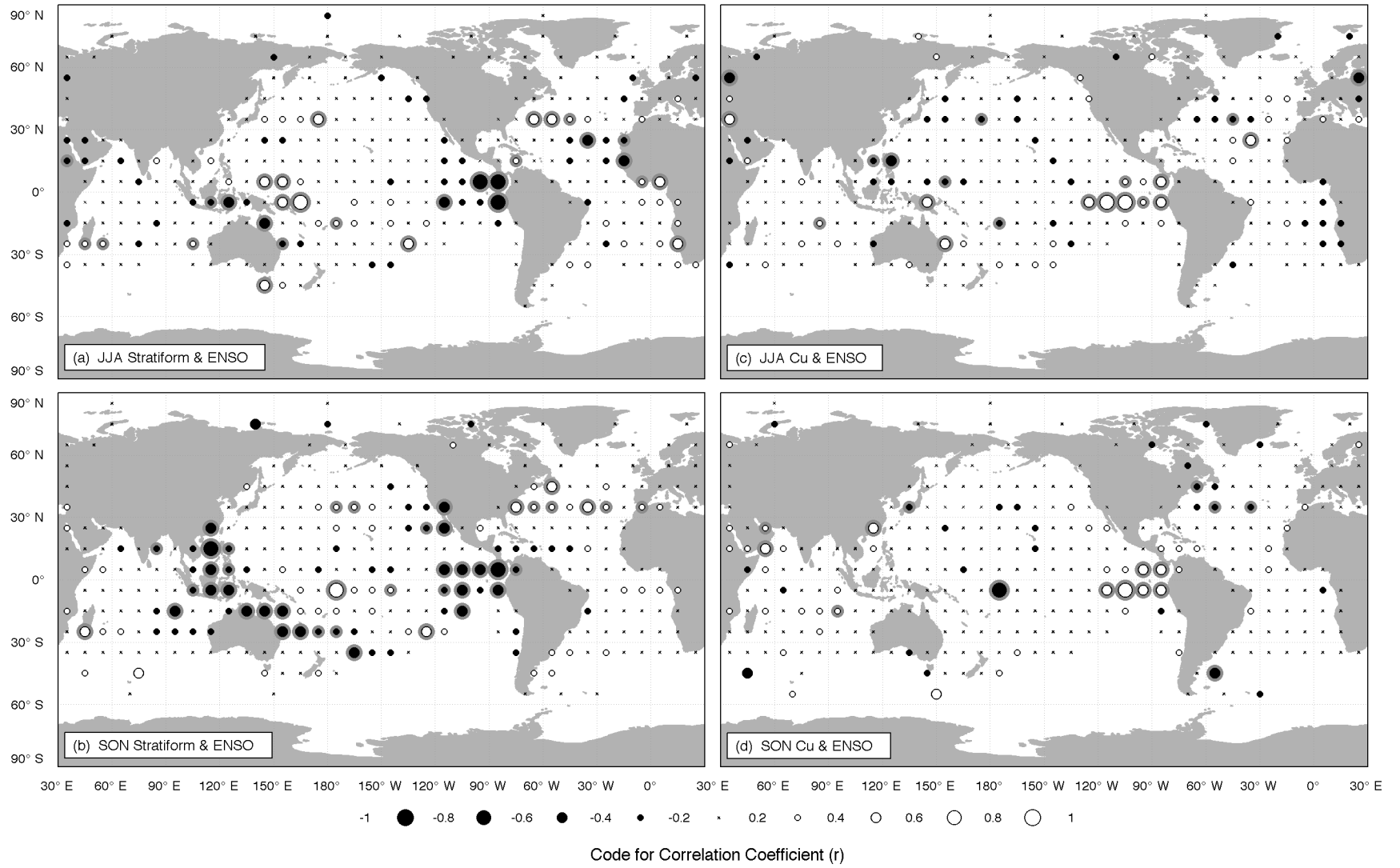


Figure 14. Linear correlations between the seasonal average ENSO index and daytime (a) stratiform cloud cover anomalies in JJA, (b) stratiform cloud cover anomalies in SON, (c) cumulus cloud cover anomalies in JJA, and (d) cumulus cloud cover anomalies in SON. Before computing the correlations, long-term variation is removed from the time series in each box using a low-pass Butterworth filter. Dots are plotted using the same scheme as Figures 9 and 12. Dots surrounded by a gray ring indicate significance at the 99% level.